Estimating the hydrogen isotopic composition of past precipitation using leaf-waxes from western Africa

James A. Collins [a,*], Enno Schefuß [a], Stefan Mulitza [a], Matthias Prange [a], Martin Werner [b], Thejna Tharammal [a], André Paul [a], Gerold Wefer [a]

[a] MARUM – Center for Marine Environmental Sciences and Faculty of Geosciences, University of Bremen, D-28359 Bremen, Germany
[b] Alfred Wegener Institute for Polar and Marine Research, D-27570 Bremerhaven, Germany

ARTICLE INFO

ABSTRACT

The hydrogen isotopic composition of plant leaf-wax n-alkanes (δD_{wax}) is a novel proxy for estimating δD of past precipitation (δD_p). However, vegetation life-form and relative humidity exert secondary effects on δD_{wax}, preventing quantitative estimates of past δD_p. Here, we present an approach for removing the effect of vegetation-type and relative humidity from δD_{wax} and thus for directly estimating past δD_p. We test this approach on modern day (late Holocene; 0–3 ka) sediments from a transect of 9 marine cores spanning 21°N–23°S off the western coast of Africa. We estimate vegetation type (C_3 tree versus C_4 grass) using $\delta^{13}C$ of leaf-wax n-alkanes and correct δD_{wax} for vegetation-type with previously-derived apparent fractionation factors for each vegetation type. Late Holocene vegetation-corrected δD_{wax} (δD_{vc}) displays a good fit with modern-day δD_p, suggesting that the effects of vegetation type and relative humidity have both been removed and thus that δD_{vc} is a good estimate of δD_p. We find that the magnitude of the effect of C_3 tree − C_4 grass changes on δD_{wax} is small compared to δD_p changes. We go on to estimate δD_{vc} for the mid-Holocene (6–8 ka), the Last Glacial Maximum (LGM; 19–23 ka) and Heinrich Stadial 1 (HS1; 16–18.5 ka). In terms of past hydrological changes, our leaf-wax based estimates of δD_p mostly reflect changes in wet season intensity, which is complementary to estimates of wet season length based on leaf-wax $\delta^{13}C$.

1. Introduction

The stable hydrogen isotopic composition (D/H ratio; expressed relative to the VSMOW standard as δD) of precipitation is a useful indicator of hydrology and climate dynamics. In the tropics it reflects both local precipitation amount and non-local rainout processes and is thus an indicator for both local- and large-scale atmospheric circulation changes. Sedimentary leaf-wax n-alkanes derived from terrestrial plants represent an archive of the hydrogen isotopic composition of past precipitation (δD_p) and are thus a useful proxy of past atmospheric dynamics. However, the interpretation of leaf-wax δD (δD_{wax}) records is complex because δD_{wax} is also affected by vegetation life-form and relative humidity (Sachse et al., 2012). Leaf-wax δD records have therefore been interpreted as reflecting past relative humidity and/or precipitation δD_p changes (Schefuß et al., 2005; Tierney et al., 2008; Niedermeyer et al., 2010), while concerns that vegetation-type changes may

dominate δD_{wax} have also been raised (Smith and Freeman, 2006; Douglas et al., 2012). A quantitative estimate of past δD_p is therefore desirable for accurate climate reconstructions. We use a new approach, using estimates of vegetation type to correct for the effect of vegetation type and relative humidity on δD_{wax}. We test this approach on modern-day (late Holocene; 0–3 ka) marine sediments from a transect of 9 well-dated, high-resolution cores. These span from 21°N to 23°S off the coast of western Africa, covering West Africa, Central Africa and southwestern Africa (Table 1, Fig. 1a). Marine sediment cores have relatively large catchment areas and thus integrate the leaf-wax signal from a large continental area. Moreover, the large scale coverage of our mapping approach provides a valuable dataset for comparison with δD_p estimates from climate models. As well as the modern day, we also analyse: the mid-Holocene (6–8 ka) to test the effect of increased northern hemisphere summer insolation; the Last Glacial Maximum (19–23 ka) to test the effect of glacial conditions and Heinrich Stadial 1 (16–18.5 ka) to test the effect of Atlantic meridional overturning circulation slowdown on African climate. These time periods can be compared with climate modelling experiments.

* Corresponding author.
E-mail address: jcollins@marum.de (J.A. Collins).

Table 1
Core transect off western Africa.

| Figure label	Region	Core number	Latitude	Longitude	Water depth (m)
1	West	GeoB7920-2	20° 45.09′ N	18° 34.90′ W	2278
2	West	GeoB9508-5	15° 29.90′ N	17° 56.88′ W	2384
3	West	GeoB9526-5	12° 26.10′ N	18° 03.40′ W	3223
4	West	GeoB9535-4	8° 52.54′ N	14° 57.66′ W	669
5	Central	GeoB4905-4	2° 30.00′ N	9° 23.40′ E	1328
6	Central	GeoB6518-1	5° 35.30′ S	11° 13.30′ E	962
7	Central	ODP1078C	11° 55.27′ S	13° 24.02′ E	500
8	Southwestern	GeoB1023-5	17° 09.43′ S	11° 00.70′ E	1978
9	Southwestern	MD08-3167	23° 18.91′ S	12° 22.61′ E	1948

2. Background

2.1. Spatial pattern of precipitation in West, Central and southwestern Africa

Most of the rain falling in tropical Africa is delivered by large convective storms known as mesoscale convective systems (Mohr and Zipser, 1996; Mohr et al., 1999; Nesbitt et al., 2006). Uplift required to create this convective rainfall is associated with the convergence of trade winds at the Intertropical Convergence Zone (West and Central Africa) and Congo Air Boundary (Central and southwestern Africa) and also with ascending air between the African Easterly Jet and Tropical Easterly Jet streams (Nicholson and Grist, 2003). These features, which collectively form the rainbelt,

oscillate latitudinally along with the seasonal insolation maximum (Nicholson and Grist, 2003). The rainbelt oscillates between extremes of ∼17°N in Jun–Jul–Aug (Fig. 1a) and ∼21°S in Dec–Jan–Feb (Fig. 1c). In West and Central Africa, moisture for convective rainfall originates mostly from the Atlantic Ocean (Fig. 1a, b, d) and in southwestern Africa from the Indian Ocean (Fig. 1c; Rouault et al., 2003; Gimeno et al., 2010). Moisture is also recycled from the continent (either evaporated from soils and lakes or transpired from leaves; Peters and Tetzlaff, 1988; Taupin et al., 2000; Gimeno et al., 2010). The Sahara and Namib Deserts receive very little monsoonal precipitation. However, coastal fog, associated with cold upwelled waters (e.g. Olivier and Stockton, 1989), is common in Namibia and is an important source of moisture for plants (Louw and Seeley, 1980; Lancaster et al., 1984; Eckardt et al., in press). The wet season (which we define as the period of the year when rainfall is greater than 5 cm per month) is longest in the Congo Basin and Guinea coast regions (these regions experience two wet seasons per year) and decreases towards the desert regions. The wet season is most intense in the coastal Guinea and Cameroon regions and this is associated with topography, proximity to moisture source and the perpendicular orientation of winds to the coast (Hayward and Oguntoyinbo, 1987; Sall et al., 2007).

2.2. Temporal and spatial pattern of modern-day precipitation δD
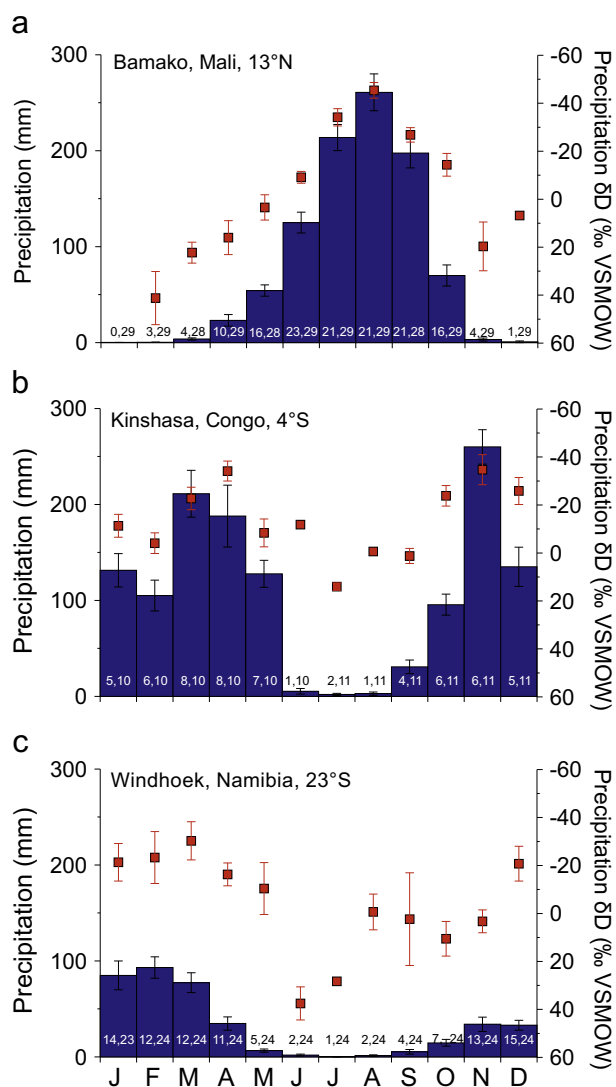
In the tropics, the hydrogen isotopic composition of precipitation is dominated by the amount effect (Dansgaard, 1964; Rozanski
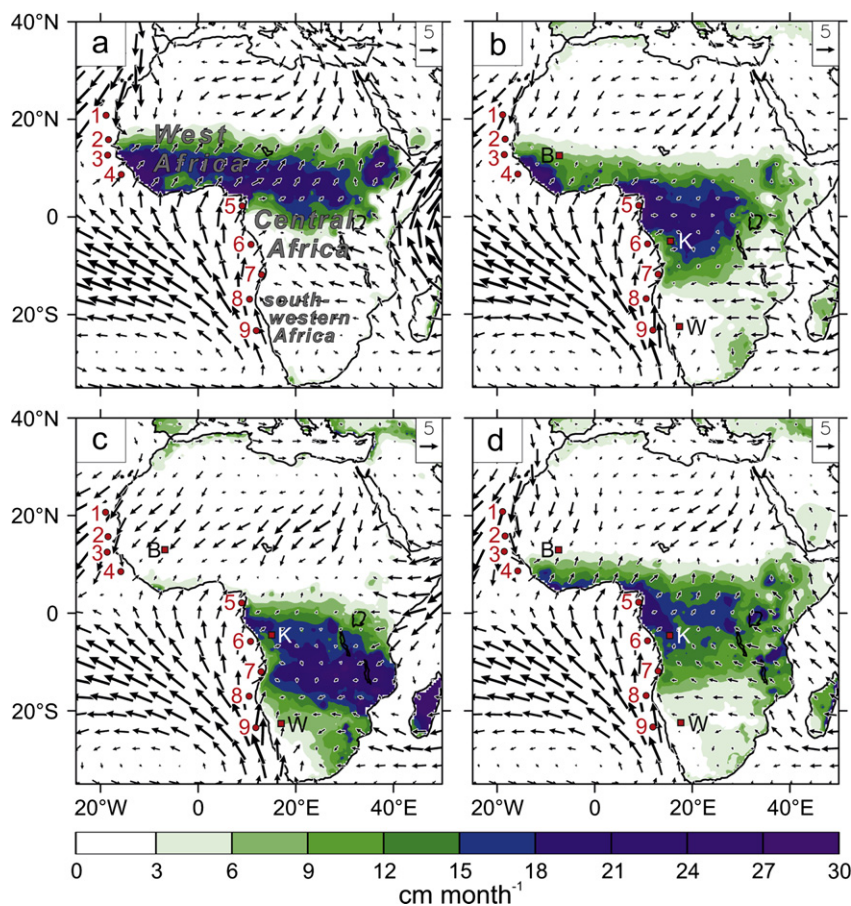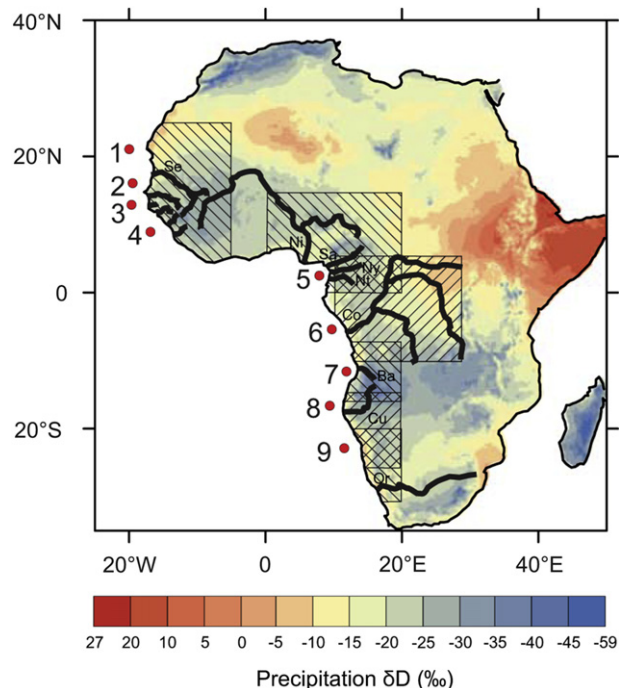

Fig. 1. Modern-day climatology of Africa, highlighting the position of the rainbelt and dominant surface wind systems during a) JJA (boreal summer), b) SON (boreal autumn), c) DJF (boreal winter) and d) MAM (boreal spring). The wind reference arrow refers to 5 m/s. Wind data are from the NCEP reanalysis (Kalnay et al., 1996) and precipitation data are from the University of Delaware dataset (climate.geog.udel.edu/∼climate). Numbered red circles mark the sediment cores used in this study (Table 1). Red squares mark the three GNIP stations referred to in the text and in Fig. 2: Bamako, B; Kinshasa, K; and Windhoek, W. (For interpretation of the references to colour in this figure legend, the reader is referred to the web version of this article.)

et al., 1993). This is a negative correlation between monthly precipitation amount and precipitation δD (δD_p). The seasonal trend in monthly precipitation amount and δD_p associated with the passage of the rainbelt is illustrated for three GNIP (Global Network for Isotopes in Precipitation; IAEA/WMO, 2006) stations in West (Bamako), Central (Kinshasa) and southwestern (Windhoek) Africa (Figs. 1b–d, 2). In terms of the amount effect, more depleted isotopes are attributed to a) reduced evaporation of falling raindrops under a moister atmosphere and b) to downward advection of isotopically depleted water vapour from high altitudes during intense convective activity, which is then used in successive convection (Risi et al., 2008a; Risi et al., 2010a). Due to the mean residence time of water vapour in the atmosphere, the δD_p integrates convective activity (intensity and frequency of storms) of the previous ~10 days (Risi et al., 2008b).

Spatially, however there is relatively poor correspondence of precipitation-weighted mean-annual δD_p (Fig. 3) with wet season

Fig. 3. Reconstructed precipitation-weighted mean-annual δD_p for Africa, based on the interpolated dataset of Bowen and Revenaugh (2003). Sediment cores are numbered (1–9). Major African rivers are marked: Senegal (Se); Niger (Ni); Sanaga (Sa); Nyong (Ny); Ntem (Nt); Congo (Co); Balombo (Ba); Cunene (Cu) and Orange (Or). Hatching marks the approximate source area of each core (Cores 1–4 are joined for clarity: see Table 2 for individual source areas). It should be noted that African GNIP stations are relatively sparsely distributed and therefore the interpolated dataset of Bowen and Revenaugh (2003) may not capture all regional isotopic variability in precipitation.

precipitation amount (Fig. 1a–d). This is because other factors exert an influence on δD_p. These include temperature during transport (altitude effect), transport distance (continental effect) and also non-local amount effect (Dansgaard, 1964; Rozanski et al., 1992; Dayem et al., 2010). These effects cause non-local rainout of an air mass and hence deplete the air mass in the heavier isotope before the moisture reaches the site of precipitation. As an example, summer δD_p is relatively depleted at the Windhoek station (Fig. 2c) even though precipitation amount is low, compared to the other stations (Fig. 2a, b). This is likely to be due to non-local rainout (Rozanski et al., 1993) during long-distance and relatively high-altitude transport from the Indian Ocean (Gimeno et al., 2010). Another factor influencing δD_p is the recycling of transpirationally-derived moisture. Moisture that is derived from plant leaf-water transpiration is thought to be unfractionated, which leads to relatively enriched δD_p values in subsequent precipitation (Salati et al., 1979; Rozanski et al., 1993; Levin et al., 2009). Densely vegetated regions such as the Congo rainforest are thought to contribute a large amount of transpirationally derived moisture (Levin et al., 2009).

2.3. Leaf-wax n-alkane δD as a recorder of precipitation δD

Long-chain, odd-numbered *n*-alkanes are produced by vascular plants (Eglinton and Hamilton, 1967) to protect the leaf cuticle (Koch and Ensikat, 2008) and are well preserved in sediments (Schimmelmann et al., 1999; Yang and Huang, 2003). The main control on spatial variations of δD_{wax} is source-water δD (δD_p; Sachse et al., 2004; Sachse et al., 2012).

Biosynthesis of *n*-alkanes induces a large negative isotopic fractionation and thus leaf-wax δD is normally negatively offset

Fig. 2. Seasonal cycle of precipitation amount (blue bars) and δD_p (red squares) for GNIP stations (IAEA/WMO, 2006) in a) West Africa (Bamako), b) Central Africa (Kinshasa) and c) southwestern Africa (Windhoek). Errors represent standard error, and the number of monthly δD_p observations followed by the number of monthly precipitation observations (n) is marked at the bottom of each figure. (For interpretation of the references to colour in this figure legend, the reader is referred to the web version of this article.)

from δD_p. However, biosynthetic fractionation is thought to be constant for given compound classes (Sessions et al., 1999) and so does not contribute to variations in δD_{wax} values.

Relative humidity and vegetation type do, however, exert a control on leaf-wax δD. To assess the effect of relative humidity and vegetation type separately from δD_p changes, leaf wax isotopic data are commonly presented in terms of the fractionation between δD_{wax} and δD_p, known as the 'apparent fractionation' (ε). Relative humidity exerts a control on the extent of evapotranspiration (and subsequent D enrichment) of soil-water and leaf-water. The effect of relative humidity has been observed in greenhouse studies (Kahmen et al., 2012a) and soil transect studies (Sachse et al., 2004; Rao et al., 2009; Kahmen et al., 2012b): in less humid environments, more soil water evaporation and transpirational leaf-water enrichment results in isotopically enriched δD_{wax} values. Vegetation type also acts to control leaf-water enrichment: C_4 grasses are thought to undergo less transpiration than C_3 trees (Sachse et al., 2012). In the natural environment, relative humidity changes may be partly counteracted by vegetation type (Hou et al., 2008): species that are less prone to evapotranspiration and leaf-water enrichment tend to thrive in arid environments. In addition to controlling the degree of leaf-water evapotranspiration, vegetation-type may control δD_{wax} in other ways such as by differences in water use efficiency (Hou et al., 2007) and rooting depth (Krull et al., 2006) and different pathways of NADPH formation (Sachse et al., 2012). In summary, δD_{wax} is the result of 3 variables: a) δD_p, b) relative humidity, and c) vegetation type (plant physiology).

2.4. Source areas and transport mechanisms of n-alkanes

Plant leaf-waxes are transported from soils to continental margin sediments along with suspended river material (Bird et al., 1995) and windblown dust (Simoneit et al., 1988). Waxes can also be directly abraded off plant leaves during dust storms (Simoneit et al., 1988) and released during biomass burning (Conte and Weber, 2002).

Although it is not possible to precisely constrain the continental catchment areas of terrestrial leaf-wax bearing material to each core, we are able to make estimates based on modern-day transport pathways, which we briefly describe below. Based on these constraints, we estimate catchment areas for each core (Table 2, Fig. 3). This allows us to derive precipitation-weighted catchment-mean δD_p values for each core (Fig. 6a), for comparison with our leaf-wax based estimates of past δD_p.

Our cores span 3 major regions in Africa: West, Central and southwestern Africa (Fig. 1a). Off West Africa, cores 1–4 (21°N–

Table 2
Estimated core-catchment areas. These are as previously estimated (Collins et al., 2011) apart from cores 5 and 8 which have been slightly modified to include some material from the Niger River (after Weldeab et al., 2011) and more material from the Namib Desert (after Eckardt and Kuring, 2005), respectively.

Core position			Catchment extent			
Number	Latitude	Longitude	Northern extent	Southern extent	Westward extent	Eastward extent
1	20.8°N	18.6°W	25.8°N	15.8°N	West coast	5°W
2	15.5°N	17.9°W	20.5°N	10.5°N	West coast	5°W
3	12.4°N	18.1°W	17.4°	7.4°N	West coast	5°W
4	8.9°N	15.0°W	13.9°N	3.9°N	West coast	5°W
5	2.5°N	9.4°E	15.0°N	0°N	0°E	20°E
6	5.6°S	11.2°E	5.0°N	10.0°S	West coast/ 10°E	30°E
7	11.9°S	13.4°E	6.9°S	16.9°S	West coast	20°E
8	17.2°S	11.0°E	15.0°S	25.0°S	West coast	20°E
9	23.3°S	12.4°E	20.0°S	30.0°S	West coast	20°E

Table 3
Age model for core MD08-3167.

Depth (cm)	Radiocarbon age (res. age uncorrected)	Std. Dev.	Calibrated age (yrs BP)
6.5	2045	30	1614
40	4880	35	5199
76	7500	40	7960
116	9290	50	10,138
216	13,190	60	15,184
312	15,920	70	18,723
420	19,630	100	22,897
515	24,740	190	29,120

9°N) receive dust that is blown westwards from the Sahara and Sahel (Goudie and Middleton, 2001) and material from West African rivers (Fig. 3). Dust storms and rivers also transport material latitudinally, the extent of which we previously estimated to be 5° of latitude (Collins et al., 2011). In terms of longitudinal extent, since most of the dust transported to the shelf originates from the Mali-Mauritania regions (Ratmeyer et al., 1999; Goudie and Middleton, 2001) and leaf-wax isotopic composition mostly reflects that of the vegetation from the latter part of a dust storm's path (Simoneit et al., 1988), we limit the eastward extent to 5°W. In Central Africa, Core 5 (3°N) receives most of its material from the Sanaga, Nyong and Ntem Rivers (Weldeab et al., 2011), some from the Niger River (likely from the lower reaches; Martins, 1982), and some dust from the Sahara (Stuut et al., 2005). Core 6 (6°S) receives mainly river sediment from the Congo River (Schefuß et al., 2005). Core 7 (12°S) receives material from the Balombo and other smaller rivers (Dupont et al., 2008) and some dust from the Namib Desert (Schefuß et al., 2003). In southwestern Africa, cores 8 and 9 (17°S and 23°S) receive most of their material as dust from the Namib/ Kalahari Deserts (Prospero et al., 2002; Eckardt and Kuring, 2005) and small amount of material from the Cunene and Orange Rivers (Bremner and Willis, 1993). Some of the dust material blown from the Namib Desert originates from the desert and some originates from the Namibian plateau (Lancaster et al., 1984; Eckardt and Kuring, 2005) and is brought into the desert by ephemeral rivers during the wet season.

3. Methods

3.1. Age models

Age models for cores 1–8 are based on published ^{14}C chronologies (Kim et al., 2002; Adegbie et al., 2003; Kim et al., 2003; Schefuß et al., 2005; Weldeab et al., 2005; Dupont et al., 2008; Mulitza et al., 2008; Zarriess and Mackensen, 2010; Collins et al., 2011). The age model for core 9 is based on eight ^{14}C ages (Table 3). All ^{14}C ages are converted to calendar ages using the Calib 6.0 marine09.14 calibration curve which corrects for a time-dependent global ocean reservoir age of about 400 years (Stuiver et al., 2005).

3.2. Sampling

In order to be able to directly compare n-alkane δD and $\delta^{13}C$, we used the same lipid extracts for the δD analyses as was used for the published $\delta^{13}C$ measurements (Collins et al., 2011). Cores were sampled using 10 ml syringes. Individual sampling depths were chosen based on the ^{14}C chronology: we sampled the late Holocene (0–3 ka), mid-Holocene (6–8 ka), Heinrich Stadial 1 (16–18.5 ka) and the Last Glacial Maximum (19–23 ka). We verified that these time intervals capture the relevant climate events using existing

time-series studies from West (Niedermeyer et al., 2010) and Central (Schefuß et al., 2005) Africa. Two to three samples were taken from each time interval, depending on availability. The samples were taken at even temporal spacing within the timeslice interval, avoiding the boundaries of the timeslices. For example, for the mid-Holocene (6–8 ka), samples were taken at (or as close as possible to) 6.7 ka and 7.3 ka (see Supplementary Table 1 for ages and depths of samples). Apart from the samples provided in Collins et al. (2011), we also took additional samples from the youngest part of the HS1 timeslice in order to better characterise the strongest reduction in Atlantic meridional overturning. Although the mean ages of each timeslice vary slightly between cores (due to material availability), this should induce little effect on our data because the time periods themselves are relatively stable, compared to difference between time periods.

3.3. δD and δ¹³C analysis of n-alkanes

δD values of n-alkanes were measured using a Thermo Trace GC coupled via a pyrolysis reactor to a Thermo Fisher MAT 253 isotope ratio mass spectrometer (GC/IR-MS). δD values were calibrated against external H_2 reference gas. The internal standard (squalane, $\delta D = -179.9‰$) added before extraction yielded an accuracy of $0.7‰$ and a precision of $2.5‰$ on average ($n = 196$). Repeated analysis ($n = 77$) of an external standard (mixture of 12 n-alkanes) between analyses yielded a root-mean-squared accuracy of $5.1‰$ and a standard deviation of on average $3.4‰$. The H_3^+ factor had a mean of 5.32 ± 0.03 and varied between 5.27 and 5.38 throughout analyses. Samples were analysed in duplicate or triplicate. For the C_{31} n-alkane, the mean value of the standard deviation between replicates is $1.3‰$. For the additional $\delta^{13}C$ measurements of samples from core MD08-3167 we followed the same method as in Collins et al. (2011). Including additional samples, the internal standard (squalane) yielded an accuracy of $0.1‰$ and a precision of $0.5‰$ on average ($n = 222$) for the $\delta^{13}C$ measurements.

3.4. Correction of δD for global ice-volume changes

For the LGM and HS1 timeslices, we correct δD_{wax} values for the effect of global ice-volume changes on meteoric water δD values, similar to e.g. Schefuß et al. (2005) and Niedermeyer et al. (2010).

We calculate the ice-volume δD correction for each sample based on the sample age and a benthic foraminiferal oxygen isotope curve (Waelbroeck et al., 2002). The curve was interpolated to each sample age and converted to δD values using the global meteoric water line (Craig, 1961). The correction assumes that δD changes were uniform throughout the African moisture source regions. The ice-volume correction shifts LGM and HS1 δD values by approximately $-8.3‰$ and $-7.9‰$, respectively.

4. Results

4.1. Source of n-alkanes

Long-chain n-alkanes from terrestrial leaf waxes typically exhibit a dominance of odd over even homologues. This dominance is quantified by the carbon preference index (CPI) and thus any influence of mature leaf-wax n-alkanes, such as petroleum (CPI ≈ 1; Kolattukudy, 1976) can be assessed. Our data display values between 2.9 and 7.8, with a mean of 5.4 (Supplementary Table 1), indicating that our sediments underwent little or no thermal maturation (they are taken from a depth of <10 m below sea floor) and there is little influence of thermally mature organic material or contamination by petroleum.

4.2. δD_wax (not corrected for vegetation-type)

We present values for the C_{31} n-alkane since this was the most cleanly separated homologue; it is abundant in both grasses and trees (Vogts et al., 2009) and is thus most suitable for use across the core transect which spans savanna and rainforest environments. For the late Holocene (modern-day) timeslice, leaf-wax δD values (δD_{wax}) range from $-138‰$ (core 9) to $-160‰$ (core 2; Fig. 4a). From north to south, the data display two minima at cores 2–3 and cores 7–8 (Fig. 4a), at the locations of more negative values in the modern-day δD_p dataset at around 15°N–5°N and 10°N–17°S (Fig. 3). In addition, there is a gradual trend to less negative values from the north to south (Fig. 4a).

Values for past timeslices are plotted as anomalies relative to the late Holocene (Fig. 4b). For the mid-Holocene, δD_{wax} anomalies are negative (isotopically depleted relative to late Holocene) at all cores, although they are within uncertainty at cores 7–9. The
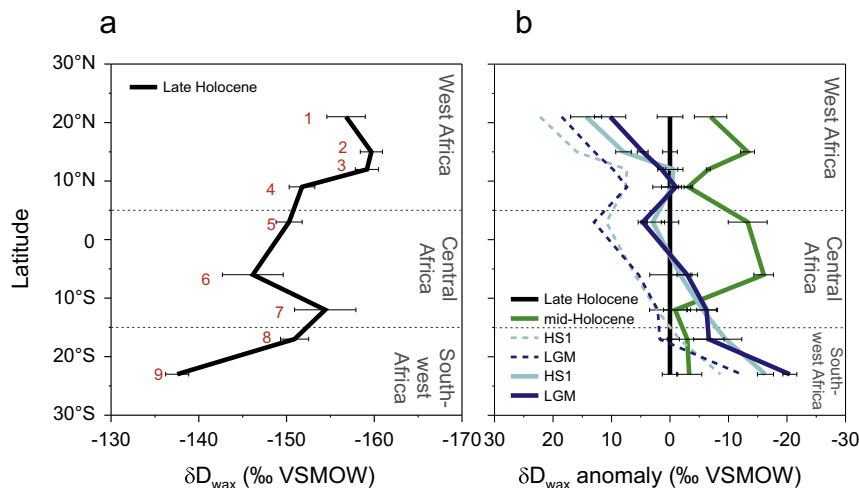
Fig. 4. (a) δD_{wax} for the late Holocene for all cores (1–9). (b) δD_{wax} for mid-Holocene (6–8 cal ka BP), Last Glacial Maximum (LGM; 19–23 cal ka BP) and Heinrich Stadial 1 (HS1; 16–18.5 cal ka BP) plotted as anomalies relative to late Holocene. Dashed lines illustrate the LGM and HS1 δD_{wax} values before ice-volume correction. Error bars (standard error) are estimated by propagating the estimated measurement reproducibility (standard deviation of replicate measurements of each sample) and the estimated variability within each timeslice (standard deviation of the samples within each timeslice).

anomalies are largest at cores 2, 5 and 6 (largest negative anomaly is −16‰). For the LGM, ice-volume corrected δD_{wax} anomalies for cores 1−6 are positive or within uncertainty (Fig. 4b). The largest positive anomaly is 10‰ (core 1). For cores 7−9, anomalies are negative and the largest negative anomaly is −20‰ (core 9). For HS1, ice-volume corrected δD_{wax} anomalies are similar to the LGM, apart from cores 1, 2 and 9, where anomalies are more positive (largest positive anomaly of 13‰ at core 1; Fig. 4b).

5. Discussion

5.1. Seasonal timing of leaf wax n-alkane formation

The seasonal timing and duration of leaf-wax n-alkane synthesis determines which part of the seasonal δD_p (Fig. 2) and evapo-transpirational cycle is recorded by the δD_{wax} values. In each of the core catchments precipitation is highly seasonal (Fig. 1), partic-ularly in semi-arid regions. Since vegetation growth is limited by water availability, almost all of the biomass (and thus most of the leaf-wax material that ends up in the soil and sediment) is pro-duced during the 'wet season' (Section 2.1). Since growth and thus wax synthesis is proportional to precipitation it is reasonable to assume that the environmental signal recorded by leaf wax is therefore weighted with precipitation.

However, studies have shown that some plant species may reflect the environmental conditions during a brief part of the wet season. For example, δD_{wax} values of field-grown barley and greenhouse-grown trees reflect the meteoric water (δD_p) and rel-ative humidity at the early stages of leaf formation (Sachse et al., 2010; Kahmen et al., 2011). This would suggest that our sedi-mentary leaf-wax n-alkanes are biased towards reflecting the start of the growing season. Conversely, however, it has also been shown that different plants (European deciduous trees) display continuous production of leaf-waxes throughout the growing season (Sachse et al., 2009). This would suggest that our sedimentary leaf-waxes reflect the isotopic composition of the latter part of the growing season, before leaf senescence (Sachse et al., 2009). However, there are as yet, no studies for African vegetation. Consequently it is not clear whether there is a bias of our sedimentary δD_{wax} signal to-wards a particular part of the wet season. We suggest, however, that the differences in seasonal timing between different species are averaged out in our sedimentary samples and as such that our

sedimentary waxes reflect a precipitation-weighted annual-mean δD. In support of this, it has been shown that environmental and physical stress can stimulate de novo leaf-wax synthesis (Shepherd and Griffiths, 2006; Gao et al., 2012): such effects might be strong in the tropics due to the intense hydrological cycle.

5.2. Pre-ageing of leaf wax n-alkanes

It has been shown that wind-blown sedimentary leaf-wax n-alkanes from West Africa are pre-aged by ∼600 years relative to the sediment (Eglinton et al., 2002). Pre-ageing is thought to be due to storage in soils and river sediments before final deposition. Pre-aged leaf waxes likely represent a mixture of ancient and young leaf waxes (Drenzek et al., 2009; Galy et al., 2011). Since pre-ageing of 600 years would not move our samples outside of our timeslices (which are 2000−4000 years in duration), pre-ageing would not affect our conclusions. It is possible, however, that the degree of pre-ageing is different in the other regions of our study area. However, at present there is no data on the degree of leaf-wax pre-ageing in Central or southwestern Africa.

Changes in the strength of the hydrological cycle could be expected to control the degree of leaf-wax pre-ageing. It is not yet known whether a stronger hydrological cycle would increase pre-ageing by eroding a greater proportion of ancient material, or whether it would decrease pre-ageing by increasing vegetation input and causing faster removal of material. However, the coeval timing of abrupt global climate changes with changes in leaf-wax n-alkane records from both West (Niedermeyer et al., 2010) and Central (Schefuß et al., 2005) Africa suggests that there is not a strong effect of pre-ageing on the climatic signal. Rather, it implies that the pool of ancient leaf-waxes incorporated into the sediment is relatively minor compared to the contribution of young material. This suggests that pre-ageing acts to slightly dampen the magni-tude of the signal, meaning that our δD_{wax} anomalies are conser-vative estimates of past climatic changes.

5.3. Correction of δD for vegetation-type

In order to remove the effect of vegetation-type from our δD_{wax} data and present vegetation-corrected values (δD_{vc}), we estimate vegetation-type changes and then remove apparent fractionation factors from our δD_{wax} values that are proportional to these
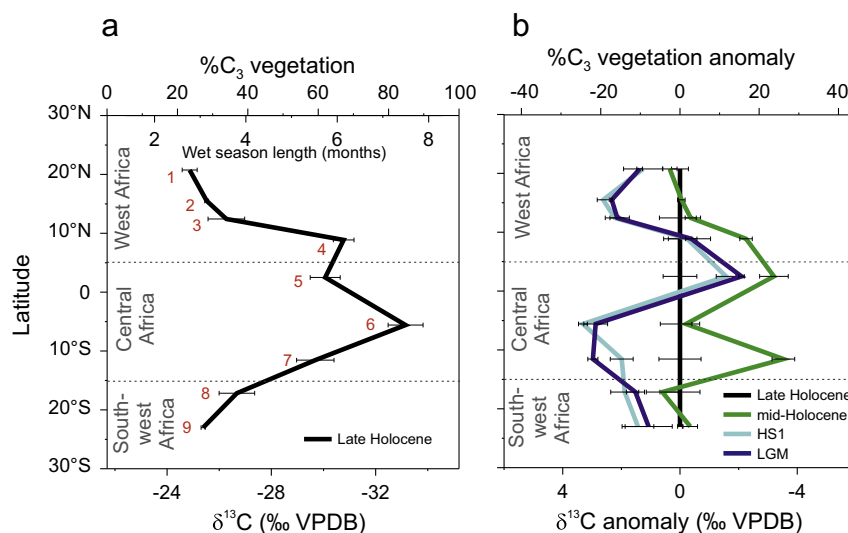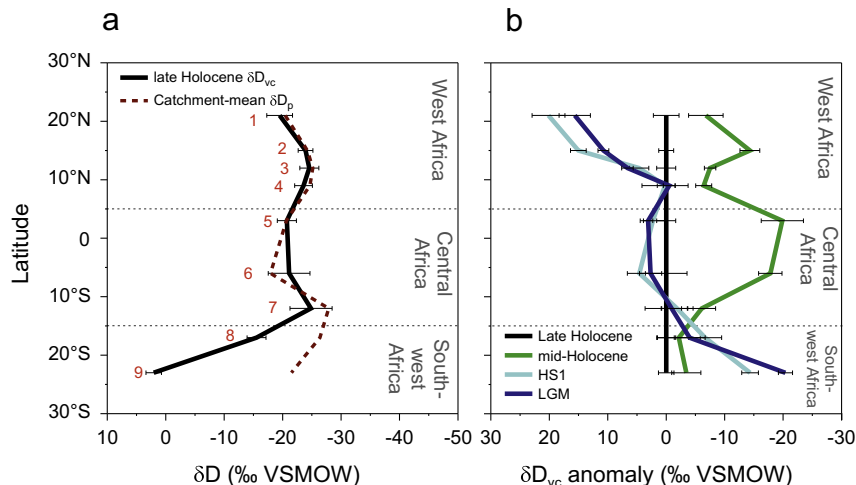

Fig. 5. (a) %C$_3$ (100-%C$_4$) vegetation in tropical western Africa for late Holocene (0−2 cal ka BP) for all cores (1−9), after Collins et al. (2011). (b) %C$_3$ vegetation for the mid-Holocene, LGM and HS1, plotted as anomalies relative to the late Holocene. Error bars (standard error) are estimated as in Fig. 4.

Fig. 6. (a) δD_{vc} for the late Holocene for all cores (1–9). Red dashed line represents the (seasonally) precipitation-weighted mean-annual δD_p for the catchment area of each core, plotted at core-site latitude. Catchment-area mean values are calculated from the Bowen and Revenaugh (2003) δD_p dataset (temporally precipitation-weighted). The catchment mean is also spatially precipitation-weighted with the University of Delaware precipitation dataset (climate.geog.udel.edu/~climate). (b) δD_{vc} for the mid-Holocene, LGM and HS1 (LGM and HS1 are ice-volume corrected), plotted as anomalies relative to the late Holocene δD_{vc} values. Error bars (standard error) are estimated by propagating the estimated measurement reproducibility (standard deviation of replicate measurements of each sample) and the estimated variability within each timeslice (standard deviation of the samples within each timeslice) and also uncertainty on the C_3–C_4 vegetation-type measurement. (For interpretation of the references to colour in this figure legend, the reader is referred to the web version of this article.)

vegetation type changes. We remove apparent fractionation factors (ε) using the formula:

$$\delta D_{vc} = [(\delta D_{wax} + 1000)/((\varepsilon/1000) + 1)] - 1000$$

In general, African vegetation types can be grouped into two end-members: C_4 grasses that thrive in semi-arid environments with a short wet season, and C_3 trees that thrive in humid environments with a longer wet season (Trochain, 1980; White, 1983; Castañeda et al., 2009; Collins et al., 2011). However, there are small amounts of C_3 grasses in the Sahara and Namib Deserts, although this is a relatively minor contribution (e.g. Edwards et al., 2010). There are also small amounts of C_3 shrubs in arid environments in Africa (Vogts et al., 2009), although again this is relatively minor. Finally, there are also some CAM plants in the Namib Desert, although the contribution is also thought to be relatively small compared to that from C_3 trees and C_4 grasses. CAM plants are mostly only abundant in the southern Namib, between 27°S and 34°S (White, 1983; Rommerskirchen et al., 2003).

We are able to estimate the proportion of C_3 trees versus C_4 grasses using $\delta^{13}C$ values of the C_{31} n-alkane (Fig. 5a,b). Although this does not account for all possible vegetation-type changes, it does account for the largest vegetation-type grouping and, since we can do this for the same samples that were used for δD_{wax} analysis, it is the most directly comparable estimate of vegetation with our δD_{wax} data, in terms of timing and source area of material.

To estimate apparent fractionation factors for the C_3 and C_4 vegetation-type end members, we select apparent fractionation factors derived from vegetation that grows in a similar climate (i.e. similar relative humidity) to that of the respective vegetation type in Africa. This may therefore act to correct for the effects of both vegetation type and relative humidity (Section 2.3). Our estimate of the apparent fractionation of C_4 grasses is based on C_4 grasses from a semi-arid environment (Great Plains, USA), which have an apparent fractionation value of $-145 \pm 15‰$ (Smith and Freeman, 2006). Our estimate for C_3 trees is based on C_3 rainforest trees (South America), which have a mean apparent fractionation value of $-125 \pm 5‰$ (Polissar and Freeman, 2010). Although these apparent fractionation factors are based on the C_{29} n-alkane, the values for the C_{31} n-alkane are very similar (Wang et al., 2012).

5.4. δD_{vc} (vegetation-type corrected)

C_4 vegetation has a more negative apparent fractionation factor ($-145‰$) and thus a larger-magnitude correction compared to C_3 vegetation ($-125‰$). Therefore the vegetation correction shifts C_4-rich regions to less negative δD_{vc} values compared to C_3-rich regions. For the late Holocene, our vegetation-corrected δD_{wax} (δD_{vc}) values range between $-25‰$ and $2‰$ (Fig. 6a). Late Holocene δD_{vc} values are in close agreement with precipitation-weighted catchment-mean δD_p for cores 1–7 (Fig. 6a). However, at cores 8 and 9, δD_{vc} values are positively offset from δD_p. The overall trend of increasing δD_{wax} values from north to south that was seen before vegetation correction (Fig. 4a) has been removed after the vegetation correction (Fig. 6a), leaving only an increase in cores 8 and 9. This suggests that the north–south increase in δD_{wax} values was mostly the result of vegetation type. The cause of the relatively positive values at cores 8 and 9 that remain after correction is discussed in Section 5.6.

For the mid-Holocene, the δD_{vc} anomaly at cores 4, 5 and 7 (Fig. 6b) is more negative relative to the δD_{wax} anomaly, due to increased C_3 vegetation at the mid-Holocene at these core sites. The overall pattern during the mid-Holocene (negative anomaly at all core sites) remains after the vegetation-type correction. The magnitude of the anomaly ranges between $-2‰$ (core 8) and $-19‰$ (core 6).

For the LGM and HS1, the δD_{vc} anomaly (Fig. 6b) at cores 1–3 and 6–9 is more positive relative to the δD_{wax} anomaly (Fig. 4b), due to increased C_4 vegetation at the LGM and HS1 in these regions. At the LGM and HS1 the δD_{vc} data still display a positive anomaly or values within uncertainty at cores 1–7 and negative anomaly at cores 8–9, which is also a similar overall pattern to before the vegetation-type correction. The magnitude of the anomaly ranges between $20‰$ (core 1) and $-20‰$ (core 9).

5.5. Magnitude of the control of vegetation-type on leaf-wax δD_{wax}

Our data suggests that the control of (C_3 tree–C_4 grass) vegetation type on δD_{wax} is relatively minor. For example, during the late Holocene, the spatial changes in vegetation type (Fig. 5a) are

different to those of δD_{wax} (Fig. 4a) and also the temporal changes in vegetation type (Fig. 5b) are different to those of δD_{wax} (Fig. 4b). In addition, the vegetation correction has a minor effect on the overall pattern of our data: the general pattern of the δD anomalies is similar before (Fig. 4b) and after (Fig. 6b) vegetation-type correction (Section 5.4). This is because a) the difference in apparent fractionation values between the C_3 and C_4 end-members is relatively small ($\sim 20\permil$) and b) the temporal changes in vegetation type at each site are relatively small (largest %C_3 anomaly is 25%; Fig. 5b). Therefore the maximum correction in our data is approximately $5\permil$, which is small compared to most of the changes in δD_{wax} between timeslices that we measured (Fig. 4b).

However this does not negate the importance of the vegetation correction because in other settings, for example, changes in %C_3 vegetation may be larger. In addition, vegetation changes other than C_3 tree–C_4 grass (with greater differences in apparent fractionation), may have taken place. For example, C_3 shrubs exhibit a smaller apparent fractionation factor ($-99\permil \pm 7\permil$) than C_4 grasses and C_3 trees (Feakins and Sessions, 2010; Sachse et al., 2012). Therefore, for C_3 shrubs the vegetation correction would be smaller in magnitude and would yield more positive δD_{vc} values. We can estimate the maximum effect that the presence of C_3 shrubs would have on our data, by assuming that the C_3 end-member is dominated by C_3 shrubs. We do this for the most arid region of our transect (core 1), where the C_3 end-member is most likely to be influenced by shrubs. C_3 shrubs exhibit a $\delta^{13}C$ composition of $-34.4\permil$ for the C_{31} n-alkane (Vogts et al., 2009), similar to C_3 trees. Based on this, we calculate the proportion of C_4 grasses versus C_3 shrubs and then re-calculate the δD vegetation-correction using the apparent fractionation for C_3 shrubs. The maximum shift towards more positive δD_{vc} values that is induced by assuming dominance of C_3 shrubs is $8\permil$ during the late Holocene. This can be considered a maximum estimate because it is unlikely that the C_3 end-member is dominated by C_3 shrubs: in reality the C_3 end-member is a mix of C_3 shrubs and C_3 trees. Overall, it is clear that specific apparent fractionation factors for the vegetation of each study region would be useful for future studies.

Finally, it has been shown that $\delta^{13}C$ values of C_3 vegetation span a relatively large range (Diefendorf et al., 2010). Thus, shifts to enriched $\delta^{13}C$ values could represent C_3 vegetation rather than a shift to C_4 vegetation. However, given that pollen data also indicate increased C_4 grasses in both northern and southern hemisphere savanna at the LGM (Dupont et al., 2000), we can assume that our $\delta^{13}C$-based estimate of vegetation-type is reasonable.

5.6. Comparison with δD_p and the effect of relative humidity on δD_{vc}

As well as vegetation type, relative humidity is thought to control δD_{wax} by causing evapotranspirational enrichment in leaf and soil waters (Sachse et al., 2004; Rao et al., 2009; Kahmen et al., 2012a, 2012b). As such, we would expect that evapotranspiration would also cause an offset (enrichment) of δD_{vc} relative to δD_p in our samples (Section 2.3), particularly in arid regions such as the Sahara–Sahel. However, this is not the case in our samples for cores 1–7 (Fig. 6a). Rather, for these cores our δD_{vc} values are closely matched with precipitation-weighted δD_p values (Fig. 6a), even in the arid Sahara–Sahel region (cores 1 and 2; 21–15°N). This suggests that evapotranspirational enrichment was already incorporated in the apparent fractionation values that we used for the vegetation correction (Section 5.3). Specifically, our C_4 grass end member was from a relatively arid environment and thus would have undergone some evapotranspirational enrichment. This was incorporated into the apparent fractionation value of $-145\permil$ that was used for the vegetation correction. Similarly, the apparent

fractionation values for tropical rainforest (Polissar and Freeman, 2010) would also incorporate the effect of evapotranspirational enrichment in this setting. Another factor contributing to the lack of an evapotranspirational signal may be the bias of leaf-wax synthesis to the wet season; the difference of wet season relative humidity between the Sahara–Sahel and equatorial regions is much smaller than the difference of annual-mean relative humidity.

In contrast to cores 1–7, δD_{vc} in southwestern Africa (cores 8–9; 17°S–23°S) is isotopically enriched compared to δD_p (Fig. 6a). We attribute this to the use of coastal fog as a moisture source by Namibian vegetation (Section 2.1). Coastal fog is isotopically enriched relative to monsoon precipitation. For example, in the western Namib Desert at 24°S, δD of fog equals $-9.5\permil$, whereas δD of groundwater derived from monsoon precipitation equals $-48.6\permil$ (Schachtschneider and February, 2010). Other estimates of monsoon precipitation δD from this region are $-24.3\permil$ (based on Windhoek GNIP station; IAEA/WMO, 2006), which is also isotopically depleted relative to fog. Therefore, we suggest that isotopically enriched fog-derived moisture biases the δD_{vc} of leaf-wax material from the Namib Desert towards values that are less negative than δD_p. The catchment-mean δD_p estimate for this region (Fig. 6a; Bowen and Revenaugh, 2003) is based on the Windhoek GNIP station data which does not incorporate (D-enriched) fog-derived moisture that is affecting the leaf-waxes.

Other explanations for the enrichment of δD_{vc} relative to δD_p could be associated with vegetation-type. In arid regions, C_3 shrubs are known to exhibit small apparent fraction factors ($-99\permil$; Section 5.5) and so it is possible that we are 'over-correcting' the δD_{wax} values from this region. However, this is unlikely to be the cause of the enrichment of δD_{vc} relative to δD_p because there is no similar offset in the Sahara, where C_3 shrubs are also known to be present (Vogts et al., 2009). CAM plants are however, relatively unique to the Namib Desert (e.g. White, 1983; Rommerskirchen et al., 2003). The contribution of CAM plants to our core is hard to determine because the leaf-wax $\delta^{13}C$ signature of CAM plants spans a relatively wide range (Chikaraishi et al., 2004). Nonetheless, it is thought that CAM plants contribute relatively little to the total biomass (Lüttge, 2004) compared to C_4 grasses, and in addition, they are concentrated in the southern Namib (White, 1983; Rommerskirchen et al., 2003). Therefore the effect on our measured δD_{vc} is likely to be relatively minor compared to the contribution from C_4 grasses. In addition, an existing study (albeit not from the Namib) suggests a fractionation factor of $-142\permil$, which is not smaller than C_4 plants (Sachse et al., 2012). Therefore we suggest that the contribution of fog moisture is the most likely explanation for the enrichment of δD_{vc} relative to δD_p values in this area.

5.7. Controls on past δD_p

Since we have accounted for changes in relative humidity and vegetation type, most of the past changes in δD_{vc} are therefore likely to have been due to past changes in δD_p. Studies have interpreted records of past δD_p as changes in local precipitation amount (Schefuß et al., 2005; Tierney et al., 2008) while modelling studies have also emphasised the importance of changes in non-local precipitation and fractionation processes (LeGrande and Schmidt, 2009; Lewis et al., 2010; Pausata et al., 2011). Non-local processes are those acting outside of the core-catchment regions to control the amount of rainout from an air mass along its path from source to site of precipitation (Section 2.2). For the timescales under consideration here they include changes in non-local precipitation amount and changes in distance to moisture source.

Temperature changes could also exert a control on δD_p. Tropical air and sea surface temperatures at the LGM were 3–5 °C lower than the late Holocene (Weijers et al., 2007; MARGO, 2009).

However a modelling study indicates that changes in the isotopic composition of precipitation at the LGM resulted from the changes in circulation and precipitation amount rather than the direct effect of temperature changes on isotopic fractionation (Risi et al., 2010b).

Changes in vegetation-type may also have controlled past δD_p by controlling the amount of transpirationally-derived moisture that is available for use in convective precipitation (Section 2.2; Levin et al., 2009). By this mechanism, the expansion of rainforest at the mid-Holocene (Fig. 5; Collins et al., 2011) would be expected to cause an increase in the proportion of moisture that is transpirationally-derived thus enrichment of δD_p. However, since our data exhibit a negative δD_{vc} anomaly at the mid-Holocene, it is unlikely that vegetation change was the major control on δD_p.

As such, the main controls on changes in past δD_p (and thus on δD_{vc}) would have been local precipitation amount, non-local precipitation amount and changes in distance to moisture source. Since our δD_{vc} values likely reflect precipitation-weighted annual-mean δD_p (Section 5.1), the amount effect component (local and non-local) likely reflects mean monthly precipitation amount during the wet season (i.e. 'wet season intensity'). As such, more negative values suggest increased wet season intensity while more positive values suggest reduced wet season intensity. This is in contrast to the use of vegetation type as a climate indicator, which is generally more sensitive to the length of the wet season ('wet season length'; Trochain, 1980; Gritti et al., 2010; Collins et al., 2011).

5.8. Local versus non-local amount effect for the modern-day

We estimate the effect of local versus non-local controls on δD_p using modern-day δD_p-precipitation amount relationships. Estimates of the amount effect range between 10‰ and 13‰ per 100 mm monthly precipitation for ocean island stations (Dansgaard, 1964). In Africa, where precipitation δD also incorporates non-local amount and the continental effect, the relationship between δD_p and precipitation amount is steeper. At Bamako the relationship is −26‰ per 100 mm monthly rainfall, at Kinshasa −14‰ per 100 mm monthly rainfall and at Windhoek −48‰ per 100 mm monthly rainfall. Consequently, southwestern Africa appears to be the most strongly influenced by non-local rainout, while Central Africa seems to be the least influenced by non-local rainout.

The above relationships give us some indication of the climatic significance of the signal in terms of precipitation amount. In West Africa, the greatest magnitude δD_{vc} anomaly is 20‰ ± 4‰. Based on the δD_p-amount relationship for the Bamako GNIP station, this equates to 77 mm ± 15 mm monthly precipitation, equivalent to about 40% of modern-day monthly wet season precipitation. In Central Africa, the greatest magnitude anomaly is −18‰ ± 4‰, which equates to 129 mm ± 29 mm monthly precipitation based on the Kinshasa station and is equivalent to about 80% of modern-day monthly precipitation. In southwestern Africa, the greatest magnitude anomaly is −20‰ ± 2‰, at the LGM, which equates to an increase in monthly precipitation of 42 mm ± 8 mm, based on the δD_p-amount relationship at Windhoek and is equivalent to about 50% of modern-day monthly wet season precipitation. Overall, the largest anomalies that we document would equate to large changes in monthly precipitation (40%–80% of modern day). The above calculations assume that the δD_p-amount relationships that we used for each region have been constant over time. Since this was not necessarily the case, these precipitation estimates should only be considered as an approximation, intended to highlight the climatic significance of the δD_{vc} changes.

In addition, there are a number of reasons why our proxy data are likely to be conservative estimates of the millennial-scale changes in δD_p that took place. Firstly, our timeslice approach means that we are integrating temporally by taking the mean of a timeslice. This will act to average out the most extreme values within the timeslice that would ordinarily be resolvable using a time-series approach. In addition, we integrate spatially: our sediments integrate a range of latitudes (Section 2.4) and thus a range of climate zones, which may also be acting to reduce the magnitude of the climate signal. Finally, a small contribution of ancient leaf-wax material (Section 5.2) is also likely to be attenuating the climate signal.

Although we use only a limited number of samples per timeslice, the general homogeneity of values between one timeslice of a given core and the same timeslice of an adjacent core suggests that our values are robust. Moreover, these subcontinental-scale patterns are unlikely to be explained by sediment re-distribution resulting from ocean current changes. It is thought that 3 degrees of latitude is the maximum transport distance that can be associated with ocean currents (Grousset et al., 1998) because dust particles are large and river sediments coagulate and sink relatively rapidly (Wefer and Fischer, 1993).

5.9. δD_{vc} during the mid-Holocene

The mid-Holocene (6–8 ka) was characterised by interglacial conditions and increased northern hemisphere summer insolation relative to today. Our δD_{vc} for the mid-Holocene exhibits a negative anomaly at all core sites in West and Central Africa and similar conditions in southwestern Africa. This is broadly in agreement with an isotope-enabled climate model, which suggests a δD_p anomaly of −8‰ to −24‰ across most of West and Central Africa (Risi et al., 2010b), and was attributed to increased precipitation amount. Other climate models, however, suggest a different response (Tierney et al., 2011a).

West Africa displays a negative anomaly during the mid-Holocene. At the Bamako GNIP station (Figs. 1 and 2), δD_p is partly controlled by local precipitation amount and partly by non-local rainout over the Eastern Sahel (Section 5.8; Risi et al., 2008b). As such, the negative δD_{vc} anomaly at the mid-Holocene may reflect an increase in local wet season intensity, increased non-local wet season intensity or increased distance to moisture source. In support of increased local wet season intensity, many studies indicate wetter conditions throughout West Africa during the mid-Holocene. For example, the expansion of lakes and the recharge of groundwater in the Sahara (Gasse, 2000), increased coverage of water bodies (Lézine et al., 2011) and increased input of river-derived material versus dust from the Senegal River (Mulitza et al., 2008) suggest wetter conditions during the mid-Holocene. The Oxford Lake-Level Database (Street-Perrott et al., 1989) also suggests wetter conditions throughout most of West Africa. In the Guinea Coast region, lake levels were increased at Lake Bosumtwi (6°N; Shanahan et al., 2006). Climate models also suggest increased wet season precipitation across West Africa (Braconnot et al., 2007). As such, at least part of the negative δD_{vc} anomaly must be due to increased local wet season intensity in West Africa. Further work with climate models will elucidate the other atmospheric processes represented by our δD_{vc} anomalies.

Central Africa displays the largest negative δD_{vc} anomaly. Sea surface salinity indicates increased river discharge from the Sanaga (Weldeab et al., 2007) and Congo Rivers (Schefuß et al., 2005). Climate models also suggest wetter conditions in Central Africa during the mid-Holocene (Braconnot et al., 2007). Since there is little influence of non-local rainout in this region (Section 5.8), the large negative δD_{vc} anomaly likely reflects a large increase in local wet season intensity in this region.

In southwestern Africa, our δD_{vc} data are within uncertainty of the late Holocene. Increased clay content in sediments suggests increased Cunene River discharge at the mid-Holocene (Gingele, 1996). In addition, proxies from the Namib Desert also suggest that the mid-Holocene (Chase et al., 2009) was wetter than today. In contrast, our data suggests relatively little change in wet season intensity (within uncertainty) in this region compared to the late Holocene.

Overall, the δD_{vc} data suggest that during the mid-Holocene there was an increase in wet season intensity between 21°N and 12°S. Leaf-wax $\delta^{13}C$ (Collins et al., 2011), an indicator for vegetation type, suggested an increase in wet season length between 10°N and 12°S, in agreement with other pollen data (e.g. Dupont et al., 2008; Ngomanda et al., 2009; Vincens et al., 2010). Taken together, the δD_{vc} and $\delta^{13}C$ imply that wet season intensity and wet season length have changed differently in the past. In particular, wet season intensity was more important than wet season length for the wetter conditions in the Sahel—Sahara (e.g. cores 1—3) during the mid-Holocene, while in Central Africa, both wet season intensity and wet season length increased.

5.10. δD_{vc} and hydroclimate at the LGM

The Last Glacial Maximum (LGM; 19—23 ka) was characterised by larger northern hemisphere ice sheets (Dyke et al., 2002; Svendsen et al., 2004), increased sea ice in the Southern Ocean (Gersonde et al., 2005) and lower global temperatures (e.g. MARGO, 2009). Our δD_{vc} values for the LGM display a north—south dipole pattern with positive anomalies or values within uncertainty for cores 1—7 (West and Central Africa) and negative anomalies for cores 8—9 (southwestern Africa; Fig. 6b). A similar pattern is reproduced by an isotope-enabled climate model for the LGM (Tharammal et al., 2012), although not in other climate models (Risi et al., 2010b). The difference between models may be due to the relatively low resolution of the model grids or shortcomings in the simulation of land surface processes (Risi et al., 2010b).

In West Africa, LGM δD_{vc} anomalies (Fig. 6b) are positive (cores 1—3) and within uncertainty (core 4). Reduced Senegal River discharge (Mulitza et al., 2008), and lower lake level at Lake Bosumtwi (Shanahan et al., 2006) imply drier conditions in West Africa during the LGM. Climate models also suggest that West Africa experienced reduced wet season precipitation at the LGM (Braconnot et al., 2007). Although again we cannot rule out some influence of decreased non-local amount or reduced distance to moisture source, the overall agreement of drier conditions in western West Africa suggests that part of the δD_{vc} signal must be due to reduced local wet season intensity. For the Fouta Djallon region (core 4), little change relative to the late Holocene implies that wet season intensity remained similar to today, which is different to the rest of West Africa and Central Africa.

In Central Africa (cores 5—7), LGM δD_{vc} anomalies are positive or within uncertainty of the late Holocene (Fig. 6b). Sea surface salinity records suggest reduced discharge from the Sanaga (Weldeab et al., 2007) and Congo (Schefuß et al., 2005) Rivers. Climate models also suggest drier conditions in this region (Braconnot et al., 2007). Since there is a relatively small effect of non-local rainout in this area, the data most likely reflects a small reduction in wet season intensity.

In southwestern Africa (cores 8 and 9), LGM δD_{vc} anomalies are negative (Fig. 6b). One possibility is that this represents a reduction in the proportion of fog-derived moisture available to the vegetation. The presence of fog is primarily the result of the advection of warm moist air over cold Benguela waters (e.g. Eckardt et al., in press). Benguela LGM sea surface temperatures (SSTs) were particularly cool compared to the rest of the south Atlantic, due to

stronger upwelling (MARGO, 2009), which might have increased the occurrence of fog. However, stronger upwelling may have also increased the width of the upwelling zone at the LGM, which might have decreased fog occurrence (Olivier and Stockton, 1989). The degree of land-surface cooling with respect to Benguela sea surface cooling, and thus the potential for on-land advection of fog, is not well known. Overall, the net effect of LGM conditions on the availability of fog-derived moisture is not clear.

In terms of hydroclimate, southwestern Africa presents a complicated picture for the LGM. Some studies indicate wetter conditions in southwestern Africa at the LGM. Increased delivery of river-derived material versus dust has been suggested for the LGM (Stuut et al., 2002) and terrestrial records suggest wetter conditions for the southernmost portion of southwestern Africa (Chase and Meadows, 2007). These studies invoke a northward shift of the winter rainfall as the cause of wetter conditions (Stuut et al., 2002; Chase and Meadows, 2007). However, the negative δD_{vc} anomaly suggests this not to be the case. This is because precipitation in the winter rainfall zone is isotopically enriched compared to monsoonal rainfall. For example, at Cape Town, which is located in the winter rainfall zone, long-term precipitation-weighted mean-annual δD_p is −13‰ (IAEA/WMO, 2006). In monsoonal rainfall regions, however, δD_p values are −24.3‰ (Windhoek, Namibia) and −43‰ (Menogue, Angola). Consequently, the negative δD_{vc} anomaly in our data suggests an enhancement of summer (monsoonal) rainfall rather than winter rainfall in this region at the LGM. Moreover, since winter rainfall regions are dominated by C_3 vegetation and our data indicate a decrease in C_3 vegetation in this region at the LGM (Fig. 5), this would also argue against an expansion of the winter rainfall zone into this part of the Namib Desert at the LGM.

Other studies suggest that the Namib Desert remained dry during the LGM (Lancaster, 2002). In addition, the clay composition and thus discharge from the Cunene River, north of the Namib was similar to today (Gingele, 1996). The presence of arid-adapted vegetation in southwestern Africa at the LGM (Shi et al., 1998) and reduced fluvial activity in the desert (Eitel et al., 2006) indicates drier conditions. However, slackwater deposits in the desert are interpreted as representing increased fluvial activity on the Namibian plateau at the LGM (Heine and Heine, 2002). This would have delivered more fine material to the desert for deflation during the dry season. This may therefore also explain the increase in fine material in sediment cores (Stuut et al., 2002).

Most modelling studies suggest that southwestern Africa was drier at the LGM (Kim et al., 2008; Tharammal et al., 2012). In southeastern Africa, however, modelling studies indicate an increase in precipitation (Kim et al., 2008; Tharammal et al., 2012) at the LGM. In addition, proxy records from southeastern Africa (Tierney et al., 2011b; Wang et al., 2012) also suggest relatively wet conditions at the LGM. In light of this, and since most moisture to southwestern Africa comes from the Indian Ocean via southeastern Africa (Gimeno et al., 2010), we interpret our depleted δD_{vc} values at the LGM to mostly reflect an increase in non-local precipitation amount (wet season intensity) over southeastern Africa. However, given that there is some evidence for a wetter Namibian plateau (Heine and Heine, 2002), the δD_{vc} anomaly may also partly represent increased local wet season intensity on the Namibian plateau. Nonetheless, the dominance of C_4 vegetation in southwestern Africa at the LGM suggests that the wet season was brief in duration, even if it was more intense. The Namib Desert itself is thought to have remained arid at the LGM (Lancaster, 2002).

Overall, the decrease in wet season intensity in West and Central Africa and the evidence for a strong increase in southeastern Africa (possibly as far West as the Namibian plateau) suggests that wet season intensity was likely shifted southeastwards at the LGM:

West and Central Africa experienced less intense wet season rainfall, while southeastern Africa experienced more intense wet season rainfall. This might reflect a southward shift of the ITCZ, which is expected to occur globally as a response to ice-sheet forcing (Kang et al., 2008). In contrast, however, our vegetation-type estimates based on leaf-wax $\delta^{13}C$ (Fig. 5) suggested a contraction of the vegetation belts and thus a contraction of wet season length towards the equator (Collins et al., 2011). Pollen data from the LGM also suggest a similar pattern (e.g. Lézine, 1989; Dupont et al., 2000; Shi et al., 2001). We suggested the vegetation pattern to be linked to a latitudinal contraction of atmospheric circulation over western Africa (Collins et al., 2011) which could have been caused by cooler SSTs in both hemispheres of the eastern tropical Atlantic (Jansen et al., 1996; MARGO, 2009; Niedermeyer et al., 2009) or by lower global temperatures (Frierson et al., 2007). The difference between the LGM vegetation-type pattern and the LGM δD_{vc} pattern seems to suggest that wet season length can change independently of wet season intensity.

5.11. δD_{vc} during Heinrich Stadial 1 (HS1)

Heinrich Stadial 1 (HS1 16–18.5 ka) is characterised by a background glacial state, with the addition of cool conditions in the North Atlantic (de Abreu et al., 2003), discharge of icebergs (Vidal et al., 1997) and a slowdown of the Atlantic meridional overturning circulation (McManus et al., 2004). In our δD_{vc} data, HS1 displays a north–south dipole, broadly similar to the LGM. Relative to the LGM, our HS1 data displays a small shift to less negative δD_{vc} in West Africa at cores 1–2 (21°N–15°N) and at core 9 (23°S). Freshwater forcing model simulations (approximate to HS1) display a positive δD_p anomaly of approximately 8‰ in West and Central Africa and a negative anomaly of approximately −8‰ in southwestern Africa (Lewis et al., 2010). Although, we see a positive anomaly in our West African δD_{vc} data, we do not see a positive anomaly in Central Africa or a negative anomaly in southwestern Africa when compared to the LGM. However, the freshwater forcing was applied to pre-industrial rather than glacial conditions and so may not be directly comparable with our data.

For West Africa, proxy records suggest reduced river versus dust input (Mulitza et al., 2008; Tjallingii et al., 2008). Freshwater forcing experiments also suggest a decrease in precipitation in the Sahel (Kageyama et al., 2009). Therefore, we interpret the positive δD_{vc} anomaly to reflect slightly reduced wet season intensity in the Sahara–Sahel region, relative to the LGM.

In Central and southwestern Africa, however, there is little change in δD_{vc} relative to the LGM, apart from at 23°S. In Central Africa other proxies also suggest similar or slightly drier hydrological conditions persisted from LGM into HS1 in Central Africa (Schefuß et al., 2005; Weldeab et al., 2007; Tierney et al., 2008). Freshwater forcing experiments also show little change in Central and southwestern Africa: the increase in precipitation only extends from South America as far as the westernmost part of the African continent (Kageyama et al., 2009). However, records from southeastern Africa suggest more positive δD_p values during HS1 (Schefuß et al., 2011; Wang et al., 2012). Via the non-local amount effect, this may explain the positive δD_{vc} anomaly (relative to the LGM) at core 9.

In addition, our $\delta^{13}C$ values did not show any major changes at HS1 relative to the LGM (Collins et al., 2011). Since HS1 is a relatively brief period it may be that we are not fully capturing the maximum 'excursion' with our timeslice approach. Another explanation may also be that the response to Heinrich Stadials is not coeval across the entire continent (Thomas et al., 2012). However, continuous records also agree that changes in Central Africa were relatively small in particular when compared to other regions, such as South America (Hessler et al., 2010). As such, we conclude

that freshwater input and ocean circulation slowdown at the HS1 was felt in West Africa, but was weakly transmitted to Central and southwestern Africa in terms of both wet season length and wet season intensity. Perhaps the lack of a response during HS1 in the Central and Southwest African regions is due to the lack of a strong SST increase in the low latitude South Atlantic at HS1 relative to the LGM (Weldeab et al., 2007; Dupont et al., 2008), compared to the strong cooling in the northeast Atlantic (de Abreu et al., 2003; Niedermeyer et al., 2009).

6. Summary and conclusions

Using the hydrogen isotopic composition of plant leaf wax n-alkanes (δD_{wax}) taken from a large-scale transect of marine sediment cores we have estimated past leaf-wax δD for West, Central and southwestern Africa. We correct our δD_{wax} values for the effect of vegetation-type (C_3 trees versus C_4 grass; estimates based on leaf wax $\delta^{13}C$) changes and find that vegetation-type has a relatively small influence on δD_{wax} values. For the late Holocene, our vegetation corrected δD (δD_{vc}) closely matches with δD_p for all regions, apart from southwestern Africa, where fog-derived moisture seems to be causing isotopic enrichment of leaf-wax δD relative to monsoon precipitation. There appears to be little effect of evapotranspiration on δD_{vc}, suggesting that it is also compensated for with the vegetation correction and thus that δD_{vc} represents an estimate of δD_p. However, the vegetation correction could be improved by a more detailed representation of vegetation changes and by specific apparent fractionation factors for African vegetation.

During the mid-Holocene, δD_{vc} anomalies are negative across the whole continent, with particularly strong changes in West and Central Africa. We interpret this to mostly reflect increased local monthly precipitation during the wet season (increased wet season intensity), although there is likely some influence of non-local processes on the signal. This suggests that increased wet season intensity was more important for hydrology than increased wet season length during the mid-Holocene in West Africa. During both the LGM and HS1, δD_{vc} anomalies are positive in West and Central Africa but negative in southwestern Africa. We interpret the positive anomalies to reflect reduced wet season intensity. In southwestern Africa, negative δD_{vc} anomalies at the LGM indicate an increase in the rainout over southeastern Africa. Overall, this suggests a southeastward shift of wet season intensity at the LGM. This is a different spatial pattern to wet season length which was reduced symmetrically about the equator at the LGM. Differences between HS1 and the LGM are small, apart from slightly more positive anomalies in West Africa which likely reflect reduced wet season intensity in this region. Overall, the use of leaf wax hydrogen and carbon isotopes in tandem is a valuable method for reconstructing both the wet season intensity and wet season length and thus understanding the dynamics of the rainbelt. Future work with water isotope-enabled climate models could investigate the importance of local and non-local processes on the isotopic composition of precipitation in Africa.

Appendix A. Supplementary data

Supplementary data related to this article can be found at http://dx.doi.org/10.1016/j.quascirev.2013.01.007.

References

Adegbie, A.T., Schneider, R.R., Röhl, U., Wefer, G., 2003. Glacial millennial-scale fluctuations in central African precipitation recorded in terrigenous sediment supply and freshwater signals offshore Cameroon. Palaeogeography, Palaeoclimatology, Palaeoecology 197, 323–333.

Bird, M.I., Summons, R.E., Gagan, M.K., Roksandic, Z., Dowling, L., Head, J., Keith Fifield, L., Cresswell, R.G., Johnson, D.P., 1995. Terrestrial vegetation change inferred from n-alkane δ^{13}C analysis in the marine environment. Geochimica et Cosmochimica Acta 59, 2853–2857.

Bowen, G.J., Revenaugh, J., 2003. Interpolating the isotopic composition of modern meteoric precipitation. Water Resources Research 39, 1299.

Braconnot, P., Otto-Bliesner, B., Harrison, S., Joussaume, S., Peterchmitt, J.Y., Abe-Ouchi, A., Crucifix, M., Driesschaert, E., Fichefet, T., Hewitt, C.D., Kageyama, M., Kitoh, A., Laine, A., Loutre, M.F., Marti, O., Merkel, U., Ramstein, G., Valdes, P., Weber, S.L., Yu, Y., Zhao, Y., 2007. Results of PMIP2 coupled simulations of the Mid-Holocene and Last Glacial Maximum – part 1: experiments and large-scale features. Climate of the Past 3, 261–277.

Bremner, J.M., Willis, J.P., 1993. Mineralogy and geochemistry of the clay fraction of sediments from the Namibian continental margin and the adjacent hinterland. Marine Geology 115, 85–116.

Castañeda, I.S., Mulitza, S., Schefuß, E., Lopes dos Santos, R.A., Sinninghe Damsté, J.S., Schouten, S., 2009. Wet phases in the Sahara/Sahel region and human migration patterns in North Africa. Proceedings of the National Academy of Sciences of the United States of America 106, 20159–20163.

Chase, B.M., Meadows, M.E., 2007. Late Quaternary dynamics of southern Africa's winter rainfall zone. Earth-science Reviews 84, 103–138.

Chase, B.M., Meadows, M.E., Scott, L., Thomas, D.S.G., Marais, E., Sealy, J., Reimer, P.J., 2009. A record of rapid Holocene climate change preserved in hyrax middens from southwestern Africa. Geology 37, 703–706.

Chikaraishi, Y., Naraoka, H., Poulson, S.R., 2004. Hydrogen and carbon isotopic fractionations of lipid biosynthesis among terrestrial (C_3, C_4 and CAM) and aquatic plants. Phytochemistry 65, 1369–1381.

Collins, J.A., Schefuß, E., Heslop, D., Mulitza, S., Prange, M., Zabel, M., Tjallingii, R., Dokken, T.M., Huang, E., Mackensen, A., Schulz, M., Tian, J., Zarriess, M., Wefer, G., 2011. Interhemispheric symmetry of the tropical African rainbelt over the past 23,000 years. Nature Geoscience 4, 42–45.

Conte, M.H., Weber, J.C., 2002. Long-range atmospheric transport of terrestrial biomarkers to the western North Atlantic. Global Biogeochemical Cycles 16, 1142.

Craig, H., 1961. Isotopic variations in meteoric waters. Science 133, 1702–1703.

Dansgaard, W., 1964. Stable isotopes in precipitation. Tellus 16, 436–468.

Dayem, K.E., Molnar, P., Battisti, D.S., Roe, G.H., 2010. Lessons learned from oxygen isotopes in modern precipitation applied to interpretation of speleothem records of paleoclimate from eastern Asia. Earth and Planetary Science Letters 295, 219–230.

de Abreu, L., Shackleton, N.J., Schönfeld, J., Hall, M., Chapman, M., 2003. Millennial-scale oceanic climate variability off the Western Iberian margin during the last two glacial periods. Marine Geology 196, 1–20.

Diefendorf, A.F., Mueller, K.E., Wing, S.L., Koch, P.L., Freeman, K.H., 2010. Global patterns in leaf ^{13}C discrimination and implications for studies of past and future climate. Proceedings of the National Academy of Sciences 107, 5738–5743.

Douglas, P.M.J., Pagani, M., Brenner, M., Hodell, D.A., Curtis, J.H., 2012. Aridity and vegetation composition are important determinants of leaf-wax δD values in southeastern Mexico and Central America. Geochimica et Cosmochimica Acta 97, 24–45.

Drenzek, N.J., Hughen, K.A., Montluçon, D.B., Southon, J.R., dos Santos, G.M., Druffel, E.R.M., Giosan, L., Eglinton, T.I., 2009. A new look at old carbon in active margin sediments. Geology 37, 239–242.

Dupont, L.M., Behling, H., Kim, J.-H., 2008. Thirty thousand years of vegetation development and climate change in Angola (Ocean Drilling Program Site 1078). Climate of the Past 4, 107–124.

Dupont, L.M., Jahns, S., Marret, F., Ning, S., 2000. Vegetation change in equatorial West Africa: time-slices for the last 150 ka. Palaeogeography, Palaeoclimatology, Palaeoecology 155, 95–122.

Dyke, A.S., Andrews, J.T., Clark, P.U., England, J.H., Miller, G.H., Shaw, J., Veillette, J.J., 2002. The Laurentide and Innuitian ice sheets during the Last Glacial Maximum. Quaternary Science Reviews 21, 9–31.

Eckardt, F.D., Kuring, N., 2005. SeaWiFS identifies dust sources in the Namib Desert. International Journal of Remote Sensing 26, 4159–4167.

Eckardt, F.D., Soderberg, K., Coop, L.J., Muller, A.A., Vickery, K.J., Grandin, R.D., Jack, C., Kapalanga, T.S., Henschel, J. The nature of moisture at Gobabeb, in the central Namib Desert. Journal of Arid Environments, in press.

Edwards, E.J., Osborne, C.P., Stromberg, C.A.E., Smith, S.A., Consortium, C.G., 2010. The origins of C_4 grasslands: integrating evolutionary and ecosystem science. Science 328, 587–591.

Eglinton, G., Hamilton, R.J., 1967. Leaf epicuticular waxes. Science 156, 1322–1335.

Eglinton, T.I., Eglinton, G., Dupont, L., Sholkovitz, E.R., Montluçon, D., Reddy, C.M., 2002. Composition, age, and provenance of organic matter in NW African dust over the Atlantic Ocean. Geochemistry Geophysics Geosystems 3, 1050.

Eitel, B., Kadereit, A., Blümel, W.-D., Hüser, K., Lomax, J., Hilgers, A., 2006. Environmental changes at the eastern Namib Desert margin before and after the Last Glacial Maximum: new evidence from fluvial deposits in the upper Hoanib River catchment, northwestern Namibia. Palaeogeography, Palaeoclimatology, Palaeoecology 234, 201–222.

Feakins, S.J., Sessions, A.L., 2010. Controls on the D/H ratios of plant leaf waxes in an arid ecosystem. Geochimica et Cosmochimica Acta 74, 2128–2141.

Frierson, D.M.W., Lu, J., Chen, G., 2007. Width of the Hadley cell in simple and comprehensive general circulation models. Geophysical Research Letters 34, L18804.

Galy, V., Eglinton, T., France-Lanord, C., Sylva, S., 2011. The provenance of vegetation and environmental signatures encoded in vascular plant biomarkers carried by the Ganges and Brahmaputra rivers. Earth and Planetary Science Letters 304, 1–12.

Gao, L., Tsai, Y.-J., Huang, Y., 2012. Assessing the rate and timing of leaf wax regeneration in Fraxinus americana using stable hydrogen isotope labeling. Rapid Communications in Mass Spectrometry 26, 2241–2250.

Gasse, F., 2000. Hydrological changes in the African tropics since the Last Glacial Maximum. Quaternary Science Reviews 19, 189–211.

Gersonde, R., Crosta, X., Abelmann, A., Armand, L., 2005. Sea-surface temperature and sea ice distribution of the Southern Ocean at the EPILOG Last Glacial Maximum – a circum-Antarctic view based on siliceous microfossil records. Quaternary Science Reviews 24, 869–896.

Gimeno, L., Drumond, A., Nieto, R., Trigo, R.M., Stohl, A., 2010. On the origin of continental precipitation. Geophysical Research Letters 37, L13804.

Gingele, F.X., 1996. Holocene climatic optimum in Southwest Africa–evidence from the marine clay mineral record. Palaeogeography, Palaeoclimatology, Palaeoecology 122, 77–87.

Goudie, A.S., Middleton, N.J., 2001. Saharan dust storms: nature and consequences. Earth-science Reviews 56, 179–204.

Gritti, E.S., Cassignat, C., Flores, O., Bonnefille, R., Chalié, F., Guiot, J., Jolly, D., 2010. Simulated effects of a seasonal precipitation change on the vegetation in tropical Africa. Climate of the Past 6, 169–178.

Grousset, F.E., Parra, M., Bory, A., Martinez, P., Bertrand, P., Shimmield, G., Ellam, R.M., 1998. Saharan wind regimes traced by the Sr-Nd isotopic composition of subtropical Atlantic sediments: Last Glacial Maximum vs today. Quaternary Science Reviews 17, 395–409.

Hayward, D.F., Oguntoyinbo, J.S., 1987. The Climatology of West Africa. Hutchinson, Barnes & Noble, London, Totowa.

Heine, K., Heine, J.T., 2002. A paleohydrologic reinterpretation of the Homeb Silts, Kuiseb River, central Namib Desert (Namibia) and paleoclimatic implications. Catena 48, 107–130.

Hessler, I., Dupont, L., Bonnefille, R., Behling, H., González, C., Helmens, K.F., Hooghiemstra, H., Lebamba, J., Ledru, M.-P., Lézine, A.-M., Maley, J., Marret, F., Vincens, A., 2010. Millennial-scale changes in vegetation records from tropical Africa and South America during the last glacial. Quaternary Science Reviews 29, 2882–2899.

Hou, J., D'Andrea, W.J., Huang, Y., 2008. Can sedimentary leaf waxes record D/H ratios of continental precipitation? Field, model, and experimental assessments. Geochimica et Cosmochimica Acta 72, 3503–3517.

Hou, J., D'Andrea, W.J., MacDonald, D., Huang, Y., 2007. Evidence for water use efficiency as an important factor in determining the δD values of tree leaf waxes. Organic Geochemistry 38, 1251–1255.

IAEA/WMO, 2006. Global Network of Isotopes in Precipitation. The GNIP Database. Accessible at: http://www.iaea.org/water.

Jansen, J.H.F., Ufkes, E., Schneider, R.R., 1996. Late Quaternary movements of the Angola-Benguela-Front, SE Atlantic, and implications for advection in the equatorial ocean. In: Wefer, G., Berger, W.H., Sidler, G., Webb, D.J. (Eds.), The South Atlantic: Present and Past Circulation. Springer-Verlag, Berlin Heidelberg, pp. 553–575.

Kageyama, M., Mignot, J., Swingedouw, D., Marzin, C., Alkama, R., Marti, O., 2009. Glacial climate sensitivity to different states of the Atlantic Meridional overturning circulation: results from the IPSL model. Climate of the Past 5, 551–570.

Kahmen, A., Dawson, T.E., Vieth, A., Sachse, D., 2011. Leaf wax n-alkane δD values are determined early in the ontogeny of Populus trichocarpa leaves when grown under controlled environmental conditions. Plant, Cell & Environment 34, 1639–1651.

Kahmen, A., Hoffmann, B., Schefuß, E., Arndt, S.K., Cernusak, L.A., West, J.B., Sachse, D., 2012b. Leaf water deuterium enrichment shapes leaf wax n-alkane δD values of angiosperm plants II: observational evidence and global implications. Geochimica et Cosmochimica Acta. http://dx.doi.org/10.1016/j.gca.2012.09.004.

Kahmen, A., Schefuß, E., Sachse, D., 2012a. Leaf water deuterium enrichment shapes leaf wax n-alkane δD values of angiosperm plants I: experimental evidence and mechanistic insights. Geochimica et Cosmochimica Acta. http://dx.doi.org/10.1016/j.gca.2012.09.003.

Kalnay, E., Kanamitsu, M., Kistler, R., Collins, W., Deaven, D., Gandin, L., Iredell, M., Saha, S., White, G., Woollen, J., Zhu, Y., Leetmaa, A., Reynolds, R., Chelliah, M., Ebisuzaki, W., Higgins, W., Janowiak, J., Mo, K.C., Ropelewski, C., Wang, J., Jenne, R., Joseph, D., 1996. The NCEP/NCAR 40-year reanalysis project. Bulletin of the American Meteorological Society 77, 437–471.

Kang, S., Held, I., Frierson, D., Zhao, M., 2008. The response of the ITCZ to extratropical thermal forcings: idealized slab ocean experiments with a GCM. Journal of Climate 21, 3521–3532.

Kim, J.-H., Schneider, R.R., Mulitza, S., Muller, P.J., 2003. Reconstruction of SE trade-wind intensity based on sea-surface temperature gradients in the Southeast Atlantic over the last 25 kyr. Geophysical Research Letters 30, 2144.

Kim, J.-H., Schneider, R.R., Müller, P.J., Wefer, G., 2002. Interhemispheric comparison of deglacial sea-surface temperature patterns in Atlantic eastern boundary currents. Earth and Planetary Science Letters 194, 383–393.

Kim, S.-J., Crowley, T., Erickson, D., Govindasamy, B., Duffy, P., Lee, B., 2008. High-resolution climate simulation of the last glacial maximum. Climate Dynamics 31, 1–16.

Koch, K., Ensikat, H.-J., 2008. The hydrophobic coatings of plant surfaces: epicuticular wax crystals and their morphologies, crystallinity and molecular self-assembly. Micron 39, 759–772.

Kolattukudy, P.E., 1976. Chemistry and Biochemistry of Natural Waxes. Elsevier Scientific Pub. Co., Amsterdam, New York.

Krull, E., Sachse, D., Mügler, I., Thiele, A., Gleixner, G., 2006. Compound-specific δ^{13}C and δ^{2}H analyses of plant and soil organic matter: a preliminary assessment of the effects of vegetation change on ecosystem hydrology. Soil Biology and Biochemistry 38, 3211–3221.

Lancaster, J., Lancaster, N., Seely, M.K., 1984. The climate of the central Namib Desert. Madoqua 14, 5–61.

Lancaster, N., 2002. How dry was dry?-Late Pleistocene palaeoclimates in the Namib Desert. Quaternary Science Reviews 21, 769–782.

LeGrande, A.N., Schmidt, G.A., 2009. Sources of Holocene variability of oxygen isotopes in paleoclimate archives. Climate of the Past 5, 441–455.

Levin, N.E., Zipser, E.J., Cerling, T.E., 2009. Isotopic composition of waters from Ethiopia and Kenya: insights into moisture sources for eastern Africa. Journal of Geophysical Research 114, D23306.

Lewis, S.C., LeGrande, A.N., Kelley, M., Schmidt, G.A., 2010. Water vapour source impacts on oxygen isotope variability in tropical precipitation during Heinrich events. Climate of the Past 6, 325–343.

Lézine, A.-M., 1989. Late quaternary vegetation and climate of the Sahel. Quaternary Research 32, 317–334.

Lézine, A.-M., Hély, C., Grenier, C., Braconnot, P., Krinner, G., 2011. Sahara and Sahel vulnerability to climate changes, lessons from Holocene hydrological data. Quaternary Science Reviews 30, 3001–3012.

Louw, G.N., Seeley, M.K., 1980. Exploitation of fog water by a Perennial Namib Dune grass, Stipagrotis Sabulicola. South African Journal of Science 76, 38–39.

Lüttge, U., 2004. Ecophysiology of crassulacean acid metabolism (CAM). Annals of Botany 93, 629–652.

MARGO, 2009. Constraints on the magnitude and patterns of ocean cooling at the Last Glacial Maximum. Nature Geoscience 2, 127–132.

Martins, O., 1982. Geochemistry of the Niger river. In: Degens, E.T. (Ed.), Transport of Carbon and Minerals in Major World Rivers: Part 1. Mitteilungen aus dem Geologisch-Paläontologischen Institut der Universität Hamburg, Hamburg, pp. 397–418.

McManus, J.F., Francois, R., Gherardi, J.M., Keigwin, L.D., Brown-Leger, S., 2004. Collapse and rapid resumption of Atlantic meridional circulation linked to deglacial climate changes. Nature 428, 834–837.

Mohr, K.I., Famiglietti, J.S., Zipser, E.J., 1999. The contribution to tropical rainfall with respect to convective system type, size, and intensity estimated from the 85-GHz ice-scattering signature. Journal of Applied Meteorology 38, 596–606.

Mohr, K.I., Zipser, E.J., 1996. Mesoscale convective systems defined by their 85-GHz ice scattering signature: size and intensity comparison over tropical oceans and continents. Monthly Weather Review 124, 2417–2437.

Mulitza, S., Prange, M., Stuut, J.B., Zabel, M., von Dobeneck, T., Itambi, A.C., Nizou, J., Schulz, M., Wefer, G., 2008. Sahel megadroughts triggered by glacial slowdowns of Atlantic meridional overturning. Paleoceanography 23, PA4206.

Nesbitt, S.W., Cifelli, R., Rutledge, S.A., 2006. Storm morphology and rainfall characteristics of TRMM precipitation features. Monthly Weather Review 134, 2702–2721.

Ngomanda, A., Chepstow-Lusty, A., Makaya, M., Favier, C., Schevin, P., Maley, J., Fontugne, M., Oslisly, R., Jolly, D., 2009. Western equatorial African forest-savanna mosaics: a legacy of late Holocene climatic change? Climate of the Past 5, 341–367.

Nicholson, S.E., Grist, J.P., 2003. The seasonal evolution of the atmospheric circulation over West Africa and equatorial Africa. Journal of Climate 16, 1013–1030.

Niedermeyer, E.M., Prange, M., Mulitza, S., Mollenhauer, G., Schefuß, E., Schulz, M., 2009. Extratropical forcing of Sahel aridity during Heinrich stadials. Geophysical Research Letters 36, L20707.

Niedermeyer, E.M., Schefuß, E., Sessions, A.L., Mulitza, S., Mollenhauer, G., Schulz, M., Wefer, G., 2010. Orbital- and millennial-scale changes in the hydrologic cycle and vegetation in the western African Sahel: insights from individual plant wax δD and δ^{13}C. Quaternary Science Reviews 29, 2996–3005.

Olivier, J., Stockton, P.L., 1989. The influence of upwelling extent upon fog incidence at Lüderitz, southern Africa. International Journal of Climatology 9, 69–75.

Pausata, F.S.R., Battisti, D.S., Nisancioglu, K.H., Bitz, C.M., 2011. Chinese stalagmite δ^{18}O controlled by changes in the Indian monsoon during a simulated Heinrich event. Nature Geoscience 4, 474–480.

Peters, M., Tetzlaff, G., 1988. The structure of West African Squall Lines and their environmental moisture budget. Meteorology and Atmospheric Physics 39, 74–84.

Polissar, P.J., Freeman, K.H., 2010. Effects of aridity and vegetation on plant-wax δD in modern lake sediments. Geochimica et Cosmochimica Acta 74, 5785–5797.

Prospero, J.M., Ginoux, P., Torres, O., Nicholson, S.E., Gill, T.E., 2002. Environmental characterization of global sources of atmospheric soil dust identified with the Nimbus 7 Total Ozone Mapping Spectrometer (TOMS) absorbing aerosol product. Reviews of Geophysics 40, 31.

Rao, Z., Zhu, Z., Jia, G., Henderson, A.C.G., Xue, Q., Wang, S., 2009. Compound specific δD values of long chain n-alkanes derived from terrestrial higher plants are indicative of the δD of meteoric waters: evidence from surface soils in eastern China. Organic Geochemistry 40, 922–930.

Ratmeyer, V., Fischer, G., Wefer, G., 1999. Lithogenic particle fluxes and grain size distributions in the deep ocean off northwest Africa: implications for seasonal changes of aeolian dust input and downward transport. Deep Sea Research Part I: Oceanographic Research Papers 46, 1289–1337.

Risi, C., Bony, S., Vimeux, F., 2008a. Influence of convective processes on the isotopic composition (δ^{18}O and δD) of precipitation and water vapor in the tropics: 2. Physical interpretation of the amount effect. Journal of Geophysical Research 113, D19306.

Risi, C., Bony, S., Vimeux, F., Chong, M., Descroix, L., 2010a. Evolution of the stable water isotopic composition of the rain sampled along Sahelian squall lines. Quarterly Journal of the Royal Meteorological Society 136, 227–242.

Risi, C., Bony, S., Vimeux, F., Descroix, L., Ibrahim, B., Lebreton, E., Mamadou, I., Sultan, B., 2008b. What controls the isotopic composition of the African monsoon precipitation? Insights from event-based precipitation collected during the 2006 AMMA field campaign. Geophysical Research Letters 35, L24808.

Risi, C., Bony, S., Vimeux, F., Jouzel, J., 2010b. Water-stable isotopes in the LMDZ4 general circulation model: model evaluation for present-day and past climates and applications to climatic interpretations of tropical isotopic records. Journal of Geophysical Research 115, D12118.

Rommerskirchen, F., Eglinton, G., Dupont, L., Güntner, U., Wenzel, C., Rullkötter, J., 2003. A north to south transect of Holocene southeast Atlantic continental margin sediments: relationship between aerosol transport and compound-specific δ^{13}C land plant biomarker and pollen records. Geochemistry Geophysics Geosystems 4, 1101.

Rouault, M., Florenchie, P., Fauchereau, N., Reason, C.J.C., 2003. South East tropical Atlantic warm events and southern African rainfall. Geophysical Research Letters 30, 8009.

Rozanski, K., Araguás-Araguás, L., Gonfiantini, R., 1992. Relation between long-term trends of Oxygen-18 isotope composition of precipitation and climate. Science 258, 981–985.

Rozanski, K., Araguás-Araguás, L., Gonfiantini, R., 1993. Isotopic patterns in modern global precipitation. In: Savin, S. (Ed.), Climate Change in Continental Isotopic Records. American Geophysical Union, Washington, DC, pp. 1–36.

Sachse, D., Billault, I., Bowen, G.J., Chikaraishi, Y., Dawson, T.E., Feakins, S.J., Freeman, K.H., Magill, C.R., McInerney, F.A., van der Meer, M.T.J., Polissar, P., Robins, R.J., Sachs, J.P., Schmidt, H.-L., Sessions, A.L., White, J.W.C., West, J.B., Kahmen, A., 2012. Molecular paleohydrology: interpreting the hydrogen-isotopic composition of lipid biomarkers from photosynthesizing organisms. Annual Review of Earth and Planetary Sciences 40, 221–249.

Sachse, D., Gleixner, G., Wilkes, H., Kahmen, A., 2010. Leaf wax n-alkane δD values of field-grown barley reflect leaf water δD values at the time of leaf formation. Geochimica et Cosmochimica Acta 74, 6741–6750.

Sachse, D., Kahmen, A., Gleixner, G., 2009. Significant seasonal variation in the hydrogen isotopic composition of leaf-wax lipids for two deciduous tree ecosystems (Fagus sylvatica and Acer pseudoplatanus). Organic Geochemistry 40, 732–742.

Sachse, D., Radke, J., Gleixner, G., 2004. Hydrogen isotope ratios of recent lacustrine sedimentary n-alkanes record modern climate variability. Geochimica et Cosmochimica Acta 68, 4877–4889.

Salati, E., Dall'Olio, A., Matsui, E., Gat, J.R., 1979. Recycling of water in the Amazon Basin: an isotopic study. Water Resources Research 15, 1250–1258.

Sall, S.M., Viltard, A., Sauvageot, H., 2007. Rainfall distribution over the Fouta Djallon – Guinea. Atmospheric Research 86, 149–161.

Schachtschneider, K., February, E.C., 2010. The relationship between fog, floods, groundwater and tree growth along the lower Kuiseb River in the hyperarid Namib. Journal of Arid Environments 74, 1632–1637.

Schefuß, E., Kuhlmann, H., Mollenhauer, G., Prange, M., Pätzold, J., 2011. Forcing of wet phases in southeast Africa over the past 17,000 years. Nature 480, 509–512.

Schefuß, E., Schouten, S., Jansen, J.H.F., Sinninghe Damste, J.S., 2003. African vegetation controlled by tropical sea surface temperatures in the mid-Pleistocene period. Nature 422, 418–421.

Schefuß, E., Schouten, S., Schneider, R.R., 2005. Climatic controls on central African hydrology during the past 20,000 years. Nature 437, 1003–1006.

Schimmelmann, A., Lewan, M.D., Wintsch, R.P., 1999. D/H isotope ratios of kerogen, bitumen, oil, and water in hydrous pyrolysis of source rocks containing kerogen types I, II, IIS, and III. Geochimica et Cosmochimica Acta 63, 3751–3766.

Sessions, A.L., Burgoyne, T.W., Schimmelmann, A., Hayes, J.M., 1999. Fractionation of hydrogen isotopes in lipid biosynthesis. Organic Geochemistry 30, 1193–1200.

Shanahan, T.M., Overpeck, J.T., Wheeler, C.W., Beck, J.W., Pigati, J.S., Talbot, M.R., Scholz, C.A., Peck, J., King, J.W., 2006. Paleoclimatic variations in West Africa from a record of late Pleistocene and Holocene lake level stands of Lake Bosumtwi, Ghana. Palaeogeography, Palaeoclimatology, Palaeoecology 242, 287–302.

Shepherd, T., Griffiths, D.W., 2006. The effects of stress on plant cuticular waxes. New Phytologist 171, 469–499.

Shi, N., Dupont, L.M., Beug, H.-J., Schneider, R., 1998. Vegetation and climate changes during the last 21 000 years in S.W. Africa based on a marine pollen record. Vegetation History and Archaeobotany 7, 127–140.

Shi, N., Schneider, R., Beug, H.-J., Dupont, L.M., 2001. Southeast trade wind variations during the last 135 kyr: evidence from pollen spectra in eastern South Atlantic sediments. Earth and Planetary Science Letters 187, 311–321.

Simoneit, B.R.T., Cox, R.E., Standley, L.J., 1988. Organic matter of the troposphere-IV. Lipids in Harmattan aerosols of Nigeria. Atmospheric Environment 22, 983–1004.

Smith, F.A., Freeman, K.H., 2006. Influence of physiology and climate on δD of leaf wax n-alkanes from C_3 and C_4 grasses. Geochimica et Cosmochimica Acta 70, 1172–1187.

Street-Perrott, F.A., Marchand, D.S., Roberts, N., Harrison, S.P., 1989. Global Lake-level Variations From 18,000 to 0 Years Ago: a Paleoclimatic Analysis, U.S. Department of Energy Technical Report 46, p. 20545, Washington, DC.

Stuiver, M., Reimer, P.J., Reimer, R.W., 2005. Calib 5.0, WWW Program and Documentation.

Stuut, J.-B., Zabel, M., Ratmeyer, V., Helmke, P., Schefuß, E., Lavik, G., Schneider, R., 2005. Provenance of present-day eolian dust collected off NW Africa. Journal of Geophysical Research 110, D04202.

Stuut, J.-B.W., Prins, M.A., Schneider, R.R., Weltje, G.J., Jansen, J.H.F., Postma, G., 2002. A 300-kyr record of aridity and wind strength in southwestern Africa: inferences from grain-size distributions of sediments on Walvis Ridge, SE Atlantic. Marine Geology 180, 221–233.

Svendsen, J.I., Alexanderson, H., Astakhov, V.I., Demidov, I., Dowdeswell, J.A., Funder, S., Gataullin, V., Henriksen, M., Hjort, C., Houmark-Nielsen, M., Hubberten, H.W., Ingólfsson, Ó., Jakobsson, M., Kjær, K.H., Larsen, E., Lokrantz, H., Lunkka, J.P., Lysá, A., Mangerud, J., Matiouchkov, A., Murray, A., Möller, P., Niessen, F., Nikolskaya, O., Polyak, L., Saarnisto, M., Siegert, C., Siegert, M.J., Spielhagen, R.F., Stein, R., 2004. Late Quaternary ice sheet history of northern Eurasia. Quaternary Science Reviews 23, 1229–1271.

Taupin, J.-D., Coudrain-Ribstein, A., Gallaire, R., Zuppi, G.M., Filly, A., 2000. Rainfall characteristics ($\delta^{18}O$, $\delta^2 H$, ΔT and ΔH_r) in western Africa: regional scale and influence of irrigated areas. Journal of Geophysical Research 105, 11911–11924.

Tharammal, T., Paul, A., Merkel, U., Noone, D., 2012. Influence of LGM boundary conditions on the global water isotope distribution in an atmospheric general circulation model. Climate of the Past Discussions 8.

Thomas, D.S.G., Burrough, S.L., Parker, A.G., 2012. Extreme events as drivers of early human behaviour in Africa? The case for variability, not catastrophic drought. Journal of Quaternary Science 27, 7–12.

Tierney, J.E., Lewis, S.C., Cook, B.I., LeGrande, A.N., Schmidt, G.A., 2011a. Model, proxy and isotopic perspectives on the East African Humid Period. Earth and Planetary Science Letters 307, 103–112.

Tierney, J.E., Russell, J.M., Huang, Y., Sinninghe Damsté, J.S., Hopmans, E.C., Cohen, A.S., 2008. Northern hemisphere controls on tropical southeast African climate during the past 60,000 years. Science 322, 252–255.

Tierney, J.E., Russell, J.M., Sinninghe Damsté, J.S., Huang, Y., Verschuren, D., 2011b. Late Quaternary behavior of the East African monsoon and the importance of the Congo Air Boundary. Quaternary Science Reviews 30, 798–807.

Tjallingii, R., Claussen, M., Stuut, J.-B.W., Fohlmeister, J., Jahn, A., Bickert, T., Lamy, F., Rohl, U., 2008. Coherent high- and low-latitude control of the northwest African hydrological balance. Nature Geoscience 1, 670–675.

Trochain, J., 1980. Ecologie vegetale de la zone intertropicale non desertique. Univ. P. Sabatier, Toulouse.

Vidal, L., Labeyrie, L., Cortijo, E., Arnold, M., Duplessy, J.C., Michel, E., Becqué, S., van Weering, T.C.E., 1997. Evidence for changes in the North Atlantic Deep Water linked to meltwater surges during the Heinrich events. Earth and Planetary Science Letters 146, 13–27.

Vincens, A., Buchet, G., Servant, M., ECOFIT Mbalang Collaborators, 2010. Vegetation response to the African Humid Period termination in central Cameroon ($7°$ N) – new pollen insight from Lake Mbalang. Climate of the Past 5, 281–294.

Vogts, A., Moossen, H., Rommerskirchen, F., Rullkötter, J., 2009. Distribution patterns and stable carbon isotopic composition of alkanes and alkan-1-ols from plant waxes of African rain forest and savanna C_3 species. Organic Geochemistry 40, 1037–1054.

Waelbroeck, C., Labeyrie, L., Michel, E., Duplessy, J.C., McManus, J.F., Lambeck, K., Balbon, E., Labracherie, M., 2002. Sea-level and deep water temperature changes derived from benthic foraminifera isotopic records. Quaternary Science Reviews 21, 295–305.

Wang, Y.V., Larsen, T., Leduc, G., Andersen, N., Blanz, T., Schneider, R.R., 2012. What does leaf wax δD from a mixed C_3/C_4 vegetation region tell us? Geochimica et Cosmochimica Acta. http://dx.doi.org/10.1016/j.gca.2012.10.016.

Wefer, G., Fischer, G., 1993. Seasonal patterns of vertical particle flux in equatorial and coastal upwelling areas of the eastern Atlantic. Deep Sea Research Part I: Oceanographic Research Papers 40, 1613–1645.

Weijers, J.W.H., Schefuß, E., Schouten, S., Damste, J.S.S., 2007. Coupled thermal and hydrological evolution of tropical Africa over the last deglaciation. Science 315, 1701–1704.

Weldeab, S., Frank, M., Stichel, T., Haley, B., Sangen, M., 2011. Spatio-temporal evolution of the West African monsoon during the last deglaciation. Geophysical Research Letters 38, L13703. http://dx.doi.org/10.1029/2011GL047805.

Weldeab, S., Lea, D.W., Schneider, R.R., Andersen, N., 2007. 155,000 years of West African monsoon and ocean thermal evolution. Science 316, 1303–1307.

Weldeab, S., Schneider, R.R., Kölling, M., Wefer, G., 2005. Holocene African droughts relate to eastern equatorial Atlantic cooling. Geology 33, 981–984.

White, F., 1983. The vegetation of Africa. Natural Resources Research 20, 1.

Yang, H., Huang, Y., 2003. Preservation of lipid hydrogen isotope ratios in Miocene lacustrine sediments and plant fossils at Clarkia, northern Idaho, USA. Organic Geochemistry 34, 413–423.

Zarriess, M., Mackensen, A., 2010. The tropical rainbelt and productivity changes off northwest Africa: a 31,000-year high-resolution record. Marine Micropaleontology 76, 76–91.